RNA Alternative Splicing and Polyadenylation and Regulation of the Glomerular Filtration Barrier

Monoj K Das[1], Amy Webb[2], Mahika Yarram[1], Christian Reilly[1], Lalith Punepalle[1], Claire Bryant[3], Rajgopal Govindarajan[4], Claire L. Moore[5], Shipra Agrawal[1]*

[1]Division of Nephrology and Hypertension, Renaissance School of Medicine, Stony Brook University, NY, USA
[2]Biomedical Informatics, The Ohio State University, Columbus, OH, USA
[3]Forge Biologics, Columbus, OH, USA
[4]Pharmaceutics and Pharmacology, The Ohio State University, Columbus, OH, USA
[5]Tufts University School of Medicine, Boston, MA, USA

Short Title: Alternative Splicing and Polyadenylation in Glomerular Disease

***Address correspondence to:**
Shipra Agrawal, Ph.D.
Division of Nephrology and Hypertension
Renaissance School of Medicine
Stony Brook University
Stony Brook, NY 11794
Fax: 631-546-7004; Phone: 631-291-8652
E-mail: shipra.agrawal@stonybrookmedicine.edu

Abstract

Background: Glomerular disease, characterized by podocyte injury and proteinuria, can lead to chronic kidney disease and end stage kidney disease. We hypothesized that the glomerular pathophysiology is associated with mRNA alternative splicing and polyadenylation of glomerular genes and of critical podocyte and slit diaphragm components that regulate the filtration barrier.

Methods: Glomerular damage, accompanied by proteinuria, was induced by puromycin-aminonucleoside or adriamycin to mimic human minimal change disease or focal segmental glomerulosclerosis (FSGS), respectively, and RNA-seq analyses was performed. Alternatively spliced and alternatively polyadenylated events through differential exon and poly(A) site usage were queried in JunctionSeq and APATrap pipelines. These events were further mapped on podocyte and glomerular landscape, analyzed and modulated for slit diaphragm components, and cis- and trans-regulatory elements were identified.

Results: Altered glomerular mRNA processing by alternative splicing/polyadenylation was identified in 136/71 and 1875/746 genes in minimal change disease and FSGS models, respectively. Transcript annotation and prioritization of significant alternative splicing and polyadenylation identified key events in several podocyte and slit diaphragm genes with novel and established roles. Alternative splicing of critical slit diaphragm components, the junction protein TJP1/ZO1 and microtubule associating protein ITM2B was further characterized. Alternative polyadenylation of core members of the slit diaphragm, *NPHS1*, *NPHS2* and NEPH1 was analyzed with potential alteration of microRNA binding sites between the proximal vs distal poly (A) site usage in their mRNAs. Concomitantly, dysregulation of trans-regulatory elements (polyadenylation and splicing factors), was discovered in these models of nephropathies. Additionally, beneficial proteinuria-reducing treatments, pioglitazone and GQ16 reversed many alternatively spliced and polyadenylated events. Moreover, GWAS SNPs as potential cis-regulatory elements were identified in several genes from the human nephrotic syndrome database. Finally, we demonstrated proof-of-concept principle of chemically modified splice switching oligonucleotides in modulating *TJP1* alternative splicing in podocytes.

Conclusion: Findings from our studies identified that glomerular pathophysiology and disruption of the filtration barrier is associated with alternative splicing and alternative polyadenylation of glomerular genes, many of which are crucial determinants of podocyte structure and function and the slit diaphragm complex.

Key Points

- Alternative mRNA processing adds an important layer of transcriptome complexity in podocyte and slit diaphragm components during glomerular injury.

- Trans- and cis- elements may offer potential mechanisms to regulate alternative splicing and polyadenylation during podocyte injury.

- Antisense oligonucleotides can regulate mRNA processing events, thus offering a potential RNA-based therapeutic strategy to treat glomerular disease.

Introduction

Glomerular disease is characterized by podocyte injury and loss, and manifests with high-grade proteinuria and additional co-morbidities[1-6]. Various forms of glomerular disease can unfortunately be refractory to existing treatments, and progress to chronic kidney disease (CKD) and end stage kidney disease[7-12]. Thus, there is a constant unmet clinical need to develop targeted therapies for glomerular disease, fueled by basic molecular studies.

Research has unraveled remarkable complexities of mRNA processing and its roles in normal cellular function and disease[13, 14]. ~95% of mammalian genes undergo alternative splicing[15], which can result in different proteins with distinct functionality. Alternative splicing also determines mRNA stability, localization, translation efficiency and micro-RNA sensitivity[16, 17]. Moreover, we and others have shown that alternative splicing is associated with many cellular processes and diseases such as differentiation, cancer, and immunity[16, 18-22]. While, there are a few reports of aberrant alternative splicing in a handful of genes relevant to CKD and glomerular disease[23], including our work on PPARγ[24], the mechanisms and role of alternative splicing in glomerulopathies is lacking.

mRNA polyadenylation is an essential maturation step in which precursor-mRNA is cleaved and trimmed at its 3'-untranslated-region (UTR) and a poly(A)-tail is added[25]. Change in the position of the poly(A) site through a process called alternative polyadenylation plays an important, increasingly appreciated role in regulation of gene expression, cellular functions and pathological processes[26-34]. Alternative polyadenylation occurs in ~70% of genes[25, 35], and shortening of the 3' UTR can remove regulatory sequences that control RNA stability, translation, and subcellular localization[26, 27, 29, 32, 33], whereas coding region shortening can dramatically alter protein function[28, 30, 31, 34]. While global changes in alternative polyadenylation have been observed in development and tumor progression, there are no reports of alternative polyadenylation in glomerulopathies.

We hypothesized that glomerular disease pathophysiology is interlinked with alternative processing of podocyte and glomerular mRNAs of key genes that regulate the filtration barrier. To study these events, we employed animal models of glomerular disease, JunctionSeq and APATrap pipelines, differentiated human podocytes and the GWAS glomerular disease database.

Methods

Animal Models

The animal studies were conducted under the approval and guidelines of the Institution Animal Care and Use Committee at Nationwide Children's Hospital. Briefly, male Wistar rats were injected intravenously (IV) with puromycin aminonucleoside (PAN, 50mg/kg) or adriamycin (7.5mg/kg) to model minimal change disease or focal segmental glomerulosclerosis (FSGS), respectively, and euthanized on Day 11 and 21 respectively, at which time kidneys were harvested and glomeruli isolated using the sequential sieving method and total RNA was isolated from the glomeruli. Kidneys were paraffin embedded and processed for histology. Serum and urine chemistry were performed on serial samples. Details are provided in the Supplementary Methods.

Additional details regarding methods and procedures, including RNASeq and Differential Expression of Genes (DEGs), JunctionSeq[36], rMATS-turbo[37] and APATrap Analyses[38], Heatmaps, Pathway Analysis and Ontology Enrichment, GWAS Correlation with alternatively spliced and alternatively polyadenylated genes, Reverse Transcriptase-Polymerase Chain Reaction (RT-PCR), 3' Rapid Amplification of cDNA Ends (RACE) Assay, Splice-Switching Oligonucleotide (SSO) Design and Assay, Western Blotting and Immunofluorescence Microscopy, and Podocyte Culture and Treatments are provided in the Supplementary Data, and in **Table 1**.

Statistics

Animal experiments were performed with n=4/group to achieve sufficient power (80%) and downstream analyses was performed after confirmation of significant proteinuria induction in both PAN and adriamycin groups. Statistical analyses were performed and adjusted p values used as described in Supplemental Data for RNASeq DEG, JunctionSeq, rMATS, APATrap data and GWAS SNPs threshold. Differentially expressed genes (DEGs) were chosen with adjusted $p<0.05$ and abs(logFC)>1<1, unless otherwise noted. All other experimental data were obtained from at least three independent experiments and expressed as mean±SEM. For UPCR, serum chemistry, qRT-PCR and densitometry analysis, one-way ANOVA or t test was used and $p<0.05$ was considered as significant.

Results

I. PAN and Adriamycin- Nephropathy Models Revealed Common and Distinct Transcriptome Signatures

Glomerular and Podocyte Injury in PAN and ADR Nephropathy Models

To study the alternative processing of glomerular mRNAs during disease, we used two well-established rat models of podocyte and glomerular injury; PAN-induced minimal change disease and adriamycin-induced FSGS) (**Figure 1A**). Proteinuria induced by IV PAN injection appeared by Day 4 and massive proteinuria was observed in adriamycin-injected rats, starting from Day 7 (**Figures 1B and C**). Histology revealed podocyte hypertrophy in the adriamycin-model and multifocal dilation of proximal tubules in both PAN and adriamycin-models (**Figure 1D)**, along with disease-related changes in serum chemistry (**Supplementary Figure S1)**.

RNA-Seq Analyses Revealed Unique and Shared Changes in Transcriptomic Landscape and Pathways in PAN and ADR Models

To gain insights into the genes and molecular pathways, we performed deep paired RNA Seq analysis from glomeruli isolated by sequential sieving method[39] from healthy and PAN and adriamycin-injured rats (Day 11 and 21, respectively). Distinct transcriptomic shifts were observed in PAN and adriamycin groups compared to controls (**Figure 1E**), and a total of 1,032 DEGs in PAN vs Control (988↑, 44↓) and 1,304 DEGs in adriamycin vs Control (1215↑, 89↓) (adj $p<0.05$ and log2FC>1<1) (**Figure 1F**). Further analysis identified common and distinct DEGs for each model (**Figure 1G**). Ontology enrichment analysis identified the top cellular components (**Figure 1Hi**), biological processes (**Figure 1Hii**), and molecular functions (**Figure 1Hiii**) for each model with unique and shared DEGs. These included extracellular matrix, actin cytoskeleton, intercellular bridges, cytokine synthesis, and components of synaptic membrane. These were further categorized by overall and ↑↓ DEGs in PAN and adriamycin models (**Supplementary Figure S2**).

Deconvolution of the transcriptome identified the contribution towards pathogenesis from a large number of genes specific to podocytes as well as other glomerular cell types, including mesangial, endothelial cells and parietal epithelial cells (**Supplementary Figure S3, Table S1**). Moreover, we identified DEGs in several established causal genes with known association with glomerular disease and podocytopathies, as well as novel genes without prior association in the transcriptome of PAN and adriamycin nephropathy models (**Supplementary Figure S4**).

II. mRNA Alternative Splicing Occurred During Glomerular Disease Pathogenesis

Glomerular mRNAs Underwent Alternative Splicing during Glomerular Injury

We used the JunctionSeq program[36] to analyze glomerular RNASeq dataset to identify differential exon usage in the PAN and adriamycin models. Glomerular injury identified a total of 136 (PAN) and 1875 (adriamycin) alternatively spliced glomerular genes vs. controls (adj $p<0.05$) (**Figure**

2A,B; Supplementary Figure S5). Among these, 104 genes were shared, while 32 and 1771 were unique to the PAN and adriamycin model, respectively. Distribution of alternative splicing events in PAN and adriamycin groups was detected using rMATS-turbo[37], with the skipped exon identified as the most prevalent type of event (**Figure 2C)**.

Robust Podocyte Metrics and Contribution from Other Glomerular Cells Identified for Alternative Splicing Events

PAN-minimal change disease and adriamycin-FSGS nephropathies are mainly characterized by podocyte injury, although other glomerular cells contribute towards pathogenesis. We deconvoluted the JunctionSeq-derived dataset by cross-referencing the significant alternative splicing with podocyte-specific transcriptomic and proteomic dataset[40], and with the glomerular top 50 most variable cell-type specific genes[41]. From the podocyte-specific transcriptomic dataset (6593 genes; TPM>10, $q<0.05$)[40], we identified 115 (PAN), 1342 (adriamycin), and 90 (PAN and adriamycin) alternatively spliced genes ($q<0.05$) (**Figure 2Di**). From the podocyte-specific iBAQ dataset (551 proteins; $q<0.05$)[40], we identified 24 (PAN), 96 (adriamycin), and 17 (PAN and adriamycin) alternatively spliced genes ($q<0.05$) (**Figure 2Dii**). Podocyte specific genes *Nphs1, Podxl1* were alternatively spliced in both disease models, while adriamycin-model presented with additional alternative splicing events in *Tmsb4x* and *Rhpn1* (**Figure 2Ei-iii**). Mesangial specific gene *Map1lc3a* was alternatively spliced in adriamycin, and a few endothelial genes were alternatively spliced in either both the models (i.e., *Flt1*), or uniquely in the adriamycin-model (i.e. *Sgk1, Adgrf5, Ehd3*). Immune cell specific gene, *Msn*, was alternatively spliced in both disease models, however, *Rpsa and B2m w*ere uniquely alternatively spliced in adriamycin. To address the diverse roles of parietal epithelial sub-types in the podocyte-regeneration and glomerular pathophysiology, we deconvoluted the significant alternative splicing events with parietal epithelial sub-populations[42]. We identified alternative splicing events in all five parietal epithelial sub-populations, with the most events clustered in the podocyte-progenitor A1 sub-population and surprisingly in the tubular-progenitors A4 sub-population, especially in the adriamycin-model (**Figure 2Fi and ii, Supplementary TableS2**).

Glomerular mRNAs Underwent Alternative Splicing in Genes with Novel and Established Roles in Glomerulopathies

In order to correlate the identified alternative splicing events in glomerular disease with genes that have established causal roles in human patients, we cross-referenced the alternatively spliced dataset with 80 monogenic glomerular disease genes[43] and 49 podocytopathy genes associated with steroid resistant nephrotic syndrome [44]. We identified 8 (PAN) and 19 (adriamycin) alternatively splicing genes with established causal roles in glomerular disease, which mostly localized within the podocytes, endothelium or glomerular basement membrane (GBM) (**Table 2a)**. Among these, 7 were common, and 14 only found in the adriamycin-model. The common genes included those localized to the podocyte membrane (*Podxl*) and cytoskeletal scaffold (*Tns2, Inf2, Itsn2*) and matrix genes in the GBM (e.g. *Lamb2* and *Col4a4*). The adriamycin-model exhibited distinct genes in the GBM (*Col4a3/5*) and in the slit diaphragm (*Nphs1*). Furthermore, comparison with genes associated with steroid resistant nephrotic syndrome identified 4 (PAN) and 15 (adriamycin) alternatively spliced

genes (**Table 2b**). In summary, our data reflects on a new mode of regulation of genes with established causal roles in human glomerular disease (**Table 2c, Supplementary TableS3**). Additionally, this study uncovered several novel genes without any prior established link to mutations in human glomerular disease, such as *Tjp1* and *Itm2b* (**Table 2d, Supplementary TableS4**).

Furthermore, we identified many of the alternative splicing events reversed with proteinuria-reducing treatments[39], Pio (60) and GQ16 (15), suggesting the potential crucial role of alternative splicing of these genes in regulating podocyte health (**Figure 2G, Supplementary Tables S5,S6**).

III. mRNA Alternative Polyadenylation Occurred During Glomerular Disease Pathogenesis

Glomerular mRNAs Underwent Alternative Polyadenylation during Glomerular Injury and a Global Shift from Proximal to Distal Poly(A) Site Usage

To dissect the role of alternative polyadenylation in podocyte and glomerular biology and pathophysiology, we applied APATrap[38] to the RNASeq datasets to identify alternatively polyadenylated mRNAs in the PAN and adriamycin-models. Glomerular injury identified alternative polyadenylation in a total of 71 (PAN) and 746 (adriamycin) glomerular genes (adj $p<0.05$) (**Figure 3A**). Among these, 55 genes were shared, while 15 were unique to the PAN model and 689 unique to the adriamycin model. A proximal to distal shift in poly(A) site usage was observed in 61 (PAN) and 715 (adriamycin) genes, and a reverse shift from distal to proximal poly(A) site usage in 10 (PAN) and 31 (adriamycin) genes, suggesting an overall lengthening of the 3'UTR in disease (**Figure 3Bi,ii**).

Robust Podocyte Metrics and Contribution from Other Glomerular Cells Identified for Alternatively Polyadenylated Events

Deconvolution of the APATrap-derived dataset by cross-referencing with the podocyte-specific transcriptomic dataset (6593 genes; TPM>10, $q<0.05$)[40], identified 55 (PAN), 567 (adriamycin) and 44 (PAN and adriamycin) alternatively polyadenylated genes ($q<0.05$) (**Figure 3Ci**). From the podocyte-specific iBAQ dataset (551 proteins; $q<0.05$)[40], we identified 11 (PAN), 48 (adriamycin) and 9 (PAN and adriamycin) alternatively polyadenylated genes ($q<0.05$) (**Figure 3Cii**). Deconvolution with glomerular cell-type dataset[41] identified <u>Podocyte</u> specific genes *Nphs1* and *Podxl1* in both models, while the adriamycin-model presented with additional alternative polyadenylation in *Nphs2* (**Figure 3Di-iii**). <u>Mesangial-</u>specific gene *Map1lc3a* and <u>endothelial</u> specific gene *Thbd* showed alternative polyadenylation in adriamycin. Deconvolution by parietal epithelial sub-populations[42] identified alternative polyadenylation events in mostly podocyte-progenitor A1 sub-population, both in PAN and adriamycin-models (**Figure 3Ei, ii, Supplementary TableS7**).

Glomerular mRNAs Underwent Alternative Polyadenylation in Genes with Novel and Established Roles in Glomerulopathies, with Varied miRNA Targeted Sites

Comparison of alternative polyadenylation-dataset in glomerular disease with 80 causal genes in human patients[43] identified 7 (PAN) and 10 (adriamycin) alternatively polyadenylated genes (**Table 3a)**. These mostly localized within the podocytes and in the slit diaphragm. Among these, 6 were

common (*Podxl, Myh9, Kirrel1/Neph1, Nphs1, Nphs2, Cd151)*, while 4 were found only in the adriamycin-model (*Dlc1, Scarb2, Wt1, Thbd*). *Lmx1b* was uniquely identified in the PAN model. Comparison with 49 podocytopathy genes associated with steroid resistant nephrotic syndrome[44] revealed 3 (PAN) and 7 (adriamycin) alternatively polyadenylated genes (**Table 3b**). In summary, our data on glomerular alternative polyadenylation in the two disease models suggested an additional layer of regulation of genes with established causal roles in human glomerular disease **(Table 3c, Supplementary Table 8)**. Additionally, this study uncovered novel genes without any prior established causal roles from human glomerular disease **(Table 3d, Supplementary Table 9)**. For each alternatively polyadenylated gene, predicted miRNA sites in the 3'UTR were identified (miRDB.org).

Furthermore, we identified many of the alternative polyadenylation events (e.g. *Kirrel1*) reversed with proteinuria-reducing treatments[39], Pio (56) and GQ-16 (20), suggesting the potential crucial role of alternative polyadenylation of these genes in regulating podocyte health (**Figure 3F, Supplementary Tables S10,S11**).

IV. *Trans-elements such as RNA Binding Proteins and Splicing and Polyadenylation Factors were Dysregulated in Glomerular Disease Models*

RNA Binding Proteins (RBPs) and Splicing Factors were Dysregulated in Glomerulopathies

Due to complete lack of information on the possible trans-regulatory roles of RBPs and splicing factors in regulating alternative splicing in podocytes, we compiled a database of ~400 RBPs that play an established role in mRNA splicing[45, 46] and cross-referenced with the DEGs (adj$p$<0.05,FC>1<1) in PAN and adriamycin-model datasets (**Figure 4Ai,ii, Supplementary TableS12**). 112 (PAN) and 155 (adriamycin) splicing factors were upregulated (96 common), including U1/2/4/5/6/11/12 small nuclear ribonucleoproteins (snRNPs), splicing factors recruited in A, B, and C complexes, specific alternative splicing factors, and RNA binding motif (RBM) proteins.

Pre-mRNA 3' Processing and Polyadenylation Factors were Dysregulated in Glomerulopathies

The molecular mechanisms underlying APA involve variations in the concentration of core 3' end processing factors and several RBPs[47]. To evaluate the contribution of these trans-elements in alternative polyadenylation events during glomerular disease, we compiled a database of core and ~209 factors of the polyadenylation machinery[47-49] and cross-referenced with the DEGs (adj$p$<0.05,FC>1<1) in PAN and adriamycin-model datasets (**Figure 4Bi,ii,iii Supplementary TableS13**). 39 (PAN) and 51 (adriamycin) polyadenylation factors were upregulated (36 common). These factors included various proteins of the pre-mRNA cleavage complex. Additional transcription and translation machinery factors were identified to be dysregulated in both the models (**Supplementary Figure S6, TableS14**).

The above data combined suggest a potential trans-regulatory mechanism of the observed alternative splicing and alternative polyadenylation events in glomerular disease models.

Additionally, cross-referencing of the GWAS signals from multi-population study (38,463 participants, 2440 cases) of SNPs associated with steroid-sensitive nephrotic syndrome (NS)[50] with

the genomic region of 136 alternatively spliced genes and 3' UTRs of 71 alternatively polyadenylated genes in the PAN-minimal change disease model dataset identified potential SNPs that may serve as cis-elements for alternative mRNA processing **(Supplementary Figure S7)**.

V. Alternative Splicing of the Core Slit Diaphragm Components TJP1 and ITM2B Revealed Downstream Alterations

Glomerular disease is characterized by podocyte injury and disruption of the slit diaphragm. TJP1/ZO1 (Tight junction protein 1), and ITM2B (Integral membrane protein 2b) have been identified as core and crucial components of the slit diaphragm[51-57]. Intrigued by the identification of these components in our alternative splicing dataset, we further validated and characterized the consequences of these events at RNA and protein level. NCBI genome browser plots of Rat *Itm2b* and *Tjp1* were constructed depicting mean normalized coverage obtained from the JunctionSeq and RNASeq datasets from control and disease groups (**Figure 5Ai, Bi**). Genomic organization of human *ITM2B* and *TJP1* gene exons show that alternative splicing of *ITM2B* uses either the 'short' (S) or the 'long' (L) Exon1, producing variants S or L (**Figure 5Aii**), and alternative splicing of *TJP1* makes variants 1 and 2 (with Ex20+ and Ex20Δ) (**Figure 5Bii**). Using primers for RT-PCR and qRT-PCR to capture alternatively spliced variants in human podocytes, a shift in the increased S/L ratio for *ITM2B* and decreased Ex20+/Δ ratio for *TJP1* was observed with injury (**Figure 5Aii,iii, 5Bii,iii**). Design and use of chemically-modified splice switching oligonucleotides (SSOs) to sterically block the Int19/Ex20 junction, was able to reduce Ex20 inclusion from ~30% to 9% in a dose dependent manner and thus modulate *TJP1* splicing (**Figure 5Bii)**. Antibodies against ITM2B captured the L form, proteolytically cleaved fragments[58] and possibly the S form (similar in size to the N-terminal cleaved fragment) (**Figure 5Aiv)**. Moreover, the L form and N terminal cleaved fragment reduced while the short-cleaved fragment increased with adriamycin injury. Antibodies against TJP1 captured the α+ (Ex20+) and αΔ (Ex20Δ) forms, showing a reduction in α+ with PAN and adriamycin injury (**Figure 5Biv)**. Furthermore, most ITM2B co-localized with α-tubulin in differentiated podocytes, indicating its association with microtubules (**Figure 5Av)**. Antibodies capturing the total (L+S) and L-specific ITM2B revealed the presence of both L and S forms in podocytes, reduction of cytosolic L form and shift of S form towards perinuclear and nuclear region during injury (**Figure 5Av)**. For TJP1, while the 20+ form expressed uniformly in the glomeruli and tubular epithelium, the 20Δ form is highly expressed in the glomeruli relative to other cells of the kidney (also seen in human protein atlas database) (**Figure 5Bv**). Moreover, a reduction was observed of the 20+ form (after accounting for adriamycin auto-fluorescence), and increase of the 20Δ form specifically at junction regions with injury, which was more pronounced with adriamycin.

Overall, these findings suggested that alternative splicing of *ITM2B* and *TJP1* resulted in different protein forms with differential localization and functions in healthy and injured podocytes.

VI. Alternative Polyadenylation of the Core Slit Diaphragm Components, NPHS1, NPHS2 and NEPH1 Revealed Differential miRNA Binding Sites

Intrigued by the identification of *Nphs1*, *Nphs2* and *Neph1 (Kirrel1)* in our alternative polyadenylation dataset, we further characterized the consequences of these events by first plotting the reads obtained in our datasets at the polyA sites (**Figure 6Ai,iii,v; Supplementary FigureS8**) and secondly with the 3' RACE and 3'UTR RT-PCR assays (**Figure 6A,ii,iv,vi**). Overall, the 3' RACE and the APAtrap analyses suggested relative distal (*Neph1* and *Nphs1*) and proximal (*Nphs2*) shifts in poly(A) site usage. Furthermore, we characterized the potential consequences of alternative poly(A) site usage by identifying miRNAs with strong binding sites between the proximal and distal poly(A) sites of *Nphs1* and *Nphs2* (**Figure 6B**).

Discussion

RNA therapeutics is a fast-evolving field, and in the past decade several pre-clinical and clinical studies have guided the potential for RNA therapies to treat different diseases[59-62]. Despite these advances, there is a considerable knowledge gap and unmet need to guide these concepts to podocytopathies. This stems from an absolute lack of understanding of mRNA processing, such as alternative splicing and alternative polyadenylation in glomerular pathophysiology. We utilized two well-established models of glomerular disease for minimal change disease and FSGS, to decipher the transcriptomic landscape at the level of the constitution and heterogeneity of mRNAs due to alternative splicing and alternative polyadenylation, beyond the transcript quantification. We identified several alternatively spliced and alternatively polyadenylated events, which potentially offer critical layers of gene regulation. Such events have been recognized as important steps in cellular development, normal physiology, and in pathological processes in other diseases[13, 14, 19-22, 26-34]. However, this is the first study to probe these mechanisms in podocyte biology and glomerulopathies. A few recent studies have highlighted the role of alternative splicing in proximal tubules in diabetic nephropathy[63], and in kidney development[64], but there is no precedence of investigating global alternative splicing and alternative polyadenylation in glomerular disease.

Transcriptomic and the alternative splicing and alternative polyadenylation profiles of minimal change disease model (PAN) and FSGS model (Adriamycin) revealed numerous previously unrecognized molecular alterations to mRNAs in the glomeruli, with differential contribution from podocytes, mesangial and endothelial cells and parietal epithelial subtypes. Moreover, while both glomerular disease types are common causes of idiopathic NS in pediatric and adult population, and are characterized by podocyte injury, they have different disease pathologies, etiologies, disease course and treatment outcome[65, 66]. FSGS, usually presents as a more severe form of treatment-resistant disease, and this was reflected in transcriptomic, alternative splicing and alternative polyadenylation profiles in the current study, as the adriamycin model exhibited more robust alterations. However, despite obvious distinct differences between the two models, we identified many overlapping genes, pathways and alternative splicing and alternative polyadenylation events, which indicated shared underlying mechanisms, and added strength to the notion that these disease forms might be different manifestations of the same progressive disease[67].

We identified a reversal of many of the alternatively spliced and alternatively polyadenylated events with treatment modalities, Pio and GQ16, which we have previously demonstrated to be beneficial in reducing proteinuria and glomerular injury[39, 68, 69]. This suggested a pathogenic or adaptive role of these events, in addition to an associative role, although future studies are warranted. Additionally, we observed concomitant dysregulation of numerous RBPs, suggesting their trans-regulatory effects on alternative splicing and alternative polyadenylation. Of particular interest was the identification of alternative splicing (*TJP1/ZO1, ITM2B*) and alternative polyadenylation (*NPHS1, NPHS2, NEPH1*) events in podocyte and slit diaphragm genes, which are critical components of the filtration barrier. Podocyte-specific deletion of *Tjp1* has been shown to result in impaired foot process interdigitation, slit diaphragm formation, and glomerular dysfunction[70], but there are is no indication of the role of *TJP1* variants (α+/α−) in podocytes[71], despite their differential epithelial distribution[72],

and recently documented importance in stress fiber assembly in another system[73]. ITM2B is a newly identified crucial transmembrane member of the Nephrin and Neph1 interactome and of slit diaphragm[51], a differential microtubular S vs L interactome of ITM2B has been recently identified in retina[74], and the loss of its N terminal domain in the S form potentially lacks the transmembrane domain. Our study for the first time demonstrated the altered expression and localization of TJP1 α+ and α– and *ITM2B* S and L forms during podocyte injury. Additionally, we demonstrated altered proximal vs distal poly(A) site usage in *Neph1, Nphs1* and *Nphs2* and potential consequences for microRNA accessibility. Shortening vs lengthening of transcripts due to proximal vs distal polyA site usage has been reported to be variable in other diseases or during differentiation[49, 75-77]. The above described alternative splicing and alternative polyadenylation events point towards a novel and previously uninvestigated mechanisms of regulation of the podocyte and slit diaphragm structure and function (**Figure 6C**). Finally, we have demonstrated the ability of chemically-modified SSO designed for steric blocking, with enhanced stability and efficacy[78], to modulate an alternative splicing event in podocytes, which provides proof-of-concept to treat glomerulopathies via slit diaphragm mRNA regulation. Notably, such technology paved the way to clinical trials and FDA-approved drugs such as nusinersen (SPINSRAZA®) for exon inclusion in Spinal Muscular Atrophy [78, 79].

There were various strengths and limitations to our study. We utilized well-established models of glomerular disease which mimic human minimal change disease and FSGS remarkably well[80], and identified critical components of the slit diaphragm and filtration barrier that exhibit alternative splicing and alternative polyadenylation events. Further validation of these targets and identification in human biopsies will provide technical and biological confirmation. However, in addition to high cost, these studies require precise probes and fresh samples to capture the differential variants. It is also critical to validate such targets in human samples or cell lines (as we have done for alternative splicing of TJP1 and ITM2B in the present study), as alternative processing events can be highly species specific[81-83]. A critical barrier is the use of bioinformatics approaches to align and stitch segments of exons, junctions and 3'UTRs to identify targets. For example, we identified differential exon usage in *NPHS1*, *NPHS2* and *PODXL* mRNAs, and evidence from other studies suggests that these podocyte genes indeed exist in spliced forms [84-87]. However, future studies are needed to understand the functional consequences of these events. Another barrier lies in the fact that often multiple alternative processing events occur on the same transcript, but with conventional RNA-seq approaches, it is not possible to link these events. While we utilized effective and proven approaches at high read depth[36, 38], new technologies such as long-readSeq, performed with sufficient depth, could provide more complete characterization of mRNA isoforms. Another limitation is that bulk glomerular RNASeq is not effective in delineating cell-specific events, in capturing alternative polyadenylation and alternative splicing in lowly-expressed genes, or in precisely mapping polyA sites, which requires 3'-end focused sequencing approaches. Future use of scRNASeq, if done at sufficient depth, will allow assignment of mRNA alternative polyadenylation events to specific cell types, but would likely not reveal many alternative splicing events due to the shortness of the reads[88-91]. Nevertheless, we have successfully deconvoluted the RNASeq data to robust podocyte-metrics and to glomerular cell-types[41, 42]. Moreover, spatial transcriptomics using probes unique for a specific mRNA isoform could also help map alternative splicing and alternative polyadenylation events to specific cell types.

In summary, the analyses of mRNA alternative splicing and alternative polyadenylation in minimal change disease and FSGS models in the present study provides novel insights and mechanisms of glomerular pathophysiology and development of novel therapeutic intervention strategies.

Acknowledgments

We thank The Ohio State University (OSU) Genomics Core Resources for RNA Sequencing Services and the College of Veterinary Medicine for Clinical Pathology Services. We also thank Rachel Cianciolo from Niche Diagnostics for Pathology Services, Neelu Singh for assistance with PAS staining of kidney slides and Research Histology Core at Stony Brook University. We also thank Matthew Sampson, MD and Michelle McNulty at Harvard Medical School for helping us with accessing the GWAS database from their published studies. These studies were partly supported by the Dialysis Clinic Inc. Award, SUNY Seed Grant Award, and NIH R01 DK133440 Award to SA. This project was also partly supported by funding from the Center for Clinical and Translational Science Genomics Shared Resource Voucher Support to SA which was supported by the NIH Clinical and Translational Science award to The Ohio State University (UL1TR002733) from the National Center for Advancing Translational Sciences, United States.

Author Contributions

MKD performed experiments, analyzed and interpreted the data, prepared figures and tables, and drafted parts of the manuscript. AW and LP performed bioinformatics analyses, prepared figures and tables, and drafted parts of the manuscript. MY, CY and CB performed experiments and prepared figures and tables. RG and CM participated in study design, data interpretation and manuscript editing. SA conceptualized and designed the study, analyzed and interpreted the data, prepared figures and tables, drafted and edited the manuscript, and acquired funding. All the authors approve of the final version of the manuscript. Part of these findings were presented at the 14th International Podocyte Conference, held at University of Pennsylvania, Philadelphia, PA in 2023, at the ASN-Kidney Week held in Philadelphia, PA in 2023, and at the RNA Society Annual Meeting held in Edinburgh, Scotland in 2024.

Conflicts of Interest

None. A provisional patent application has been filed.

Data Sharing

RNA-Seq data has been deposited to the Gene Expression Omnibus (GEO) data repository:
GSE179945 and GSE286014

Figure Legends

Figure 1

Puromycin amino-nucleoside (PAN)- and adriamycin (ADR)- induced models of nephropathy revealed common and distinct transcriptome signatures in glomerulopathies. **(A)** Schematic for PAN and adriamycin (ADR)-induced nephropathy models showing a single IV injection of **(Ai)** PAN (50 mg/kg) and **(Aii)** adriamycin (ADR) (7.5 mg/kg) in male Wistar rats resulted in **(B)** induction of proteinuria and increased urinary protein/creatinine ratio (UPCR) compared to healthy controls. PAN: 35.83 mg/mg ± SEM 16.47 mg/mg, Day 11; Adriamycin (ADR): 88.31 mg/mg ± SEM 16.95 mg/mg, Day 21. **(C)** Representative urine gels showing temporal increase in albumin bands in both PAN and adriamycin (ADR) models. **(D)** Periodic acid schiff (PAS) stained images (10X and 40X) of the kidney cortex of a representative rat from each group: **(Di)** control, **(Dii)** PAN- induced nephropathy, and **(Diii)** adriamycin (ADR)- induced nephropathy. Normal kidney parenchyma was observed in healthy controls. In contrast, PAN- and adriamycin (ADR)-injured rats displayed multifocal dilation of proximal tubules due to the presence of intraluminal protein casts, with a much higher increase with adriamycin (ADR) injury. At the observed timepoints there were no visible histologic glomerular changes in the PAN model (Day 11) In the adriamycin (ADR) rats (Day 21), many of the glomeruli showed marked hypertrophy of podocytes with prominent intracytoplasmic vacuolation. At least 10 glomerular fields were observed per rat (n=4) per group. Scale bar 50 µm, 40X images and 100 µm, 10X images. **(E)** RNA Seq followed by Principal Component analysis (PCA) depicting a glomerular transcriptomic shift in PAN and adriamycin (ADR) groups compared to controls. Each dot represents the glomerular transcriptome of a healthy and PAN and adriamycin (ADR)-injured rat. Integrity of the glomeruli for each group is shown by representative glomerulus embedded in Histogel on the right. Scale bar 10 µm. **(F)** Venn diagram of differentially expressed genes (DEGs) observed in the glomeruli of PAN and adriamycin (ADR) models compared to healthy controls. 840 DEGs are common, 192 DEGs unique to PAN model, and 464 DEGs unique to adriamycin (ADR) model. **(G)** Common and distinct upregulated and downregulated DEGs in PAN and adriamycin (ADR) disease models. 805 genes are upregulated and 35 genes are downregulated in both PAN and adriamycin (ADR). 183 and 410 genes were distinctly upregulated, and 9 and 54 genes were distinctly downregulated in the PAN and adriamycin (ADR) models, respectively. **(H)** Ontology enrichment analysis identified the top cellular components (GOCC, **Hi**), biological processes (GOBP, **Hii**), and molecular functions (GOMF, **Hiii**) associated with each disease model for their unique DEGs and shared DEGs. (**Hi**) The cellular components of DEGs unique to adriamycin (ADR) included extracellular matrix and collagen trimer, those unique to PAN included basement membrane and synaptic membrane and of DEGs shared between the two models included actin cytoskeleton and intercellular bridges. (**Hii**) The biological processes identified from the DEGs unique to adriamycin (ADR) included extracellular matrix and collagen fibril organization and IL6 and TNFα production, those unique to PAN included regulation of nuclear division and chromosome segregation and of DEGs shared between the two models included extracellular matrix organization and collagen biosynthesis. (**Hiii**) The molecular

functions identified from the DEGs unique to adriamycin (ADR) included extracellular matrix binding and of DEGs shared between the two models included actin, integrin and microtubule binding.

Figure 2

Glomerular mRNAs were alternatively spliced (AS) in puromycin amino-nucleoside (PAN)- and adriamycin (ADR)- induced nephropathy models mimicking minimal change disease (MCD) and FSGS. **(A)** Schematic showing the experimental and JunctionSeq bioinformatic workflow to detect differential exon usage or alternatively spliced mRNA transcripts (shown as mutually exclusive exons) in the glomeruli of rats subjected to PAN- and adriamycin (ADR)-induced injury. Alternatively spliced transcripts can also be generated due to additional splicing events (such as alternative 5' and 3' splice sites usage, intron retention, exon skipping/inclusion) not depicted in the schematic. Venn diagram depicts the common and distinct alternatively spliced genes detected in both the models compared to healthy rats. **(B)** MA plots depict the relationship between normalized coverage and fold change between groups highlighting the measures that are much higher in one group than the other, observed in **(Bi)** PAN and **(Bii)** adriamycin (ADR) models. **(Ci)** Different kinds of alternative splicing events, and **(Cii)** their Distribution in PAN and Adriamycin (ADR). Pie charts illustrate the proportion of five alternative splicing event types: Skipped exon (SE), Retained intron (RI), Alternative 5' splice sites (A5SS), Alternative 3' splice sites (A3SS) and Mutually exclusive exons (MXE) detected across PAN and adriamycin (ADR) injury compared to healthy control using rMATS-turbo. The distribution highlights differences in splicing patterns, with statistically significant events selected based on an FDR threshold (≤0.05). **(D)** Podocyte metrics. **(Ci)** Podocyte-specific transcriptomic dataset of 6593 genes (TPM > 10, $q < 0.05$), identified 115 and 1342 alternatively spliced genes ($q < 0.05$) in PAN and adriamycin (ADR) models. 90 common alternatively spliced genes between the two models are in red. **(Dii)** Podocyte-specific iBAQ dataset of 551 proteins ($q < 0.05$) identified 24 and 96 alternatively spliced genes ($q < 0.05$) in PAN and adriamycin (ADR) models. 17 common alternatively spliced genes between the two models are in red. **(E)** Deconvolution distribution of alternatively spliced genes across the different glomerular cell types, including podocytes, mesangial cells, endothelial cells and a small fraction of immune cells in **(Ei)** PAN and **(Eii)** adriamycin (ADR) models. **(Eiii)** Genes from the deconvolution represented in PAN and adriamycin (ADR) models. **(F)** Deconvolution distribution of alternatively spliced genes across the different parietal epithelial cell (PEC) subtypes, including PEC-A1, PEC-A2, PEC-A3, PEC-A4 and PEC-B population, in **(Fi)** PAN and **(Fii)** adriamycin (ADR) models. **(G)** Venn Diagram showing alternatively spliced genes reversed with Pio and GQ-16 treatments in PAN model.

Figure 3

Glomerular mRNAs were alternatively polyadenylated (APA) in puromycin amino-nucleoside (PAN)- and adriamycin (ADR)- induced nephropathy models mimicking minimal change disease (MCD) and FSGS. **(Ai)** Schematic showing the experimental and APATrap bioinformatic workflow to detect APA mRNA transcripts in the glomeruli of rats subjected to PAN- and adriamycin (ADR)-induced injury. Venn diagram depicts the common and distinct alternatively polyadenylated genes

detected in both the models compared to healthy rats. **(B)** Volcano plots depict the 3'UTR length difference and a shift towards distal vs proximal poly A site usage for each of the significant alternatively polyadenylated genes observed in the **(Bi)** PAN and **(Bii)** adriamycin (ADR) model. **(C)** Podocyte metrics. **(Ci)** Podocyte-specific transcriptomic dataset of 6593 genes (TPM > 10, $q < 0.05$), identified 55 and 567 APA genes ($q < 0.05$) in PAN and adriamycin (ADR) models. 44 common APA genes between the two models are in red. **(Cii)** Podocyte-specific iBAQ dataset of 551 proteins ($q < 0.05$) identified 11 and 48 APA genes ($q < 0.05$) in PAN and adriamycin (ADR) models. 9 common alternatively polyadenylated genes between the two models are in red. **(D)** Deconvolution distribution of alternatively polyadenylated genes across the different glomerular cell types, including podocytes, mesangial cells, endothelial cells and a small fraction of immune cells in **(Di)** PAN and **(Dii)** adriamycin (ADR) models. **(Diii)** Genes from the deconvolution represented in PAN and adriamycin (ADR) models. **(E)** Deconvolution distribution of alternatively polyadenylated genes across the different parietal epithelial cell (PEC) subtypes, including PEC-A1, PEC-A2, PEC-A3, PEC-A4 and PEC-B population, in **(Ei)** PAN and **(Eii)** adriamycin (ADR) models. **(F)** Venn Diagram showing alternatively polyadenylated genes reversed with Pio and GQ-16 treatments in PAN model.

Figure 4

A multitude of splicing and polyadenylation factors, RNA binding proteins and 3' processing factors were dysregulated in the PAN and adriamycin (ADR) models of glomerular disease. **(A)** Heatmap of DEGs in the PAN and adriamycin (ADR) models represented in the dataset of ~400 splicing factors and RNA binding proteins (compiled for this study) that play an established role in mRNA splicing. **(i)** Cross-referenced with the DEGs (adj p <0.05, FC>1, <1) in the PAN RNASeq dataset, **(ii)** Cross-referenced with the DEGs (adj p <0.05, FC>1, <1) in the adriamycin (ADR) RNASeq dataset. **(B)** Heatmap of DEGs in the PAN and adriamycin (ADR) models represented in the dataset of ~209 pre-mRNA 3' processing and polyadenylation factors (compiled for this study) **(i)** Cross-referenced with the DEGs (adj p <0.05, FC>1, <1) in the PAN RNASeq dataset, **(ii)** Cross-referenced with the DEGs (adj p <0.05, FC>1, <1) in the adriamycin (ADR) RNASeq dataset. **(Biii)** "Core" polyadenylation factors cross-referenced with the DEGs (adj p <0.05, FC>1, <1) in the PAN and adriamycin (ADR) RNASeq dataset.

Figure 5

Alternative splicing (AS) of the core slit diaphragm components TJP1 and ITM2B revealed downstream alterations. **(Ai, Bi)** NCBI genome browser plots were constructed from the Rnor_6.0 primary assembly for mean normalized coverage (n=4 each group) obtained from the JuntionSeq and RNASeq datasets for glomeruli from control and adriamycin (ADR)-injured rats. Reads for each exon and junction (left y axis), and the entire gene (right y axis) is depicted for **(Ai)** *Itm2b* and **(Bi)** *Tjp1* for control (blue bars) and adriamycin (ADR)-injured glomeruli (red bars). Due to reverse gene orientation, the exon numbers are depicted in reverse. **(Aii, Bii)** Genomic organization of human *ITM2B* and *TJP1* gene exons, highlighting the alternatively spliced exons, primers, translation start and stop sites for each variant are depicted. **(Aii)** Alternative splicing of *ITM2B* makes use of either the 'short' (S) or the 'long' (L) E1, producing transcript variant forms S or L. These use different ATG

start codons, resulting in-frame but N-terminally different protein forms S and L. **(Bii)** Alternative splicing of *TJP1* gives rise to transcript variant forms 1 and 2 (with Ex20+ and Ex20Δ), which results in different, but in-frame protein forms α+ and α−. **(Aii, iii and Bii, iii)** RT-PCR and qRT-PCR assays using specific primer pairs (shown as arrows on genes) to detect L (purple arrows) and S (blue arrows) splice variant forms for *ITM2B* **(Aii)** and both Ex20+ and Ex20Δ as doublet (red arrows), or specific Ex20+ (blue arrows) and Ex20Δ (purple arrows) spliced forms for *TJP1* **(Bii)** are shown in control, PAN-injured and adriamycin (ADR)-injured human podocytes and % inclusion of variant forms calculated. *RPL6* is shown and used as the housekeeping gene. An 87 ↓ and 103% ↑ in the expression of the L variant, and an even higher 183%↑ and 155% ↑in the expression of the S form of the *ITM2B* variants was detected in PAN- and adriamycin (ADR)- injured podocytes, respectively, indicating an overall shift in ↑S/L ratio with podocyte injury. The two *TJP1* variant forms 1 and 2 (with Ex20+ and Ex20Δ), could be captured with a common primer pair and a clear reduction in the % exon 20 inclusion from 44% to 17% and 21% was observed in PAN- and adriamycin (ADR)- injured podocytes, respectively. qRT-PCR experiments for specific variants corroborated these results. Chemically modified splice switching oligonucleotides (SSO) designed to sterically block the intron 19/ exon 20 junction site was able to show reduction in Ex20 inclusion from ~30% to 8-9% in differentiated podocytes 48 hrs after transfection using Lipofectamine Ltx. The SSO sequence, modifications, complementarity and binding site on TJP1 pre-mRNA is depicted in red. **(Aiv, Biv)** Western blot assays to capture different protein forms of ITM2B and TJP1 are shown in Control, PAN (10 and 25 µg/ml, 48 hrs) and Adriamycin (ADR, 5µg/ml, 48 hrs) injured podocytes. **(Aiv)** Antibodies against total ITM2B captured the L form, cleaved fragments (ITM2B also gets proteolytically cleaved to give rise to different protein fragments in addition to L and S spliced forms) and possibly the S form (similar in size to the N-terminal Cleaved fragment). The L form and N terminal cleaved fragment reduced with adriamycin injury, while the short-cleaved fragment seems to increase in injury. The L encoded protein segment is highlighted in red in the ITM2B protein structure derived from 'Sequence coverage visualizer'. **(Biv)** Antibodies against TJP1 captured the α+ (Ex20+) and αΔ (Ex20Δ) forms, with a reduction in α+ with PAN and adriamycin injury. The Ex20 encoded protein fragment is highlighted in red in the α+ form of TJP1/ZO1 protein structure derived from 'Sequence coverage visualizer'. Antibodies able to capture the total (purple) and specific spliced forms (brown) used in the study are also shown in the schematic. The correct band sizes for ITM2B and TJP1 were estimated from fusion proteins generated in our laboratory (data not shown). **(Av, Bv)** Representative images of immunofluorescence microscopy of podocytes and glomeruli using 'total' and 'spliced form specific' antibodies against ITM2B and TJP1 are shown. **(Av)** ITM2B total (red), α-tubulin (green) and DAPI (blue) are shown in healthy differentiated human podocytes (upper panel). Scale bar 10 µm. Majority of ITM2B co-localized with α-tubulin in differentiated podocytes, indicating the association of ITM2B form with microtubules. ITM2B total (red), ITM2B L form (green) and DAPI (blue) are shown in Control, PAN (25µg/ml, 48 hours) and adriamycin (ADR, 5 µg/ml, 48 hours) injured podocytes (lower panel). Scale bar 10 µm. Both L and S forms could be detected in podocytes, with reduction of cytosolic L form and shift of S form towards nucleus during injury. Additional nuclear staining was observed due to auto-fluorescent property of adriamycin. **(Bv)** TJP1 total (green), TJP1 20+ (red) and

DAPI (blue) are shown in glomeruli from healthy rat (upper panel). Scale bar 10 µm. The 20+ form seemed to be expressed uniformly in the glomeruli and tubular epithelium, while the 20Δ form was highly expressed in the glomeruli relative to other cells of the kidney (also seen in human protein atlas database). TJP1 total (green), TJP1 20+ (red) and DAPI (blue) are shown in Control, PAN (25µg/ml, 48 hours) and adriamycin (ADR, 5 µg/ml, 48 hours) injured podocytes (lower panel). Scale bar 5 µm. A clear reduction was observed of the 20+ form (after accounting for the auto-fluorescent property of adriamycin in the nucleus), and increase of the 20Δ form specifically at junction regions with injury, which was more pronounced in Adriamycin-induced injury.

Figure 6

Alternative polyadenylation (APA) of the core slit-diaphragm components, **(Ai, ii)** *Neph1*, **(Aiii, iv)** *Nphs1*, and **(Av, vi)** *Nphs2* mRNAs. First, NCBI genome browser plots were constructed for *Neph1*, *Nphs1* and *Nphs2* using the Rnor_6.0 primary assembly and the reads obtained in our datasets were plotted at the polyA sites. Gene orientation is depicted by green arrow. The tracks show gene, terminal exon start site and polyA sites (red bars), translation stop site (red circle and bar) on the chromosome with '+' '-' gene orientation. Mean number of reads (n=4 each group) are depicted for control (grey bars) and adriamycin (ADR)-injured glomeruli (purple bars). Second, primers were designed for 3'RACE, 3'UTR RT-PCR and internal RT-PCR assays to detect the products that could result from proximal vs distal polyA site usage in the rat glomeruli of control healthy and adriamycin (ADR)-injured rats. Gels show distal bands for 3' RACE assays and RT-PCRs for 3' UTR and internal regions for each gene and housekeeping *Gapdh*. Primers are shown on the gene tracks (blue for 3' UTR PCR and red for 3' RACE assay). Semi-quantitative analysis of the distal amplification bands obtained from these reactions (confirmed by sequencing, Supplementary Data) was performed with densitometry, and these were further normalized to internal amplification bands to account for increased adaptive expression observed in all the 3 genes examined. While, *Gapdh* polyA site usage remained similar in Control and adriamycin (ADR)-injured rats, ~ 364% ↑ (P=0.02) in *Neph1* distal band, a trend of ~ 365% ↑ in *Nphs1* distal band, and a trend of ~ 70% ↓ in *Nphs2* distal band was detected. Overall, the 3' RACE and the APAtrap analyses suggested relative distal (lengthening of *Neph1* and *Nphs1* mRNAs) and proximal (shortening of *Nphs2* mRNA) shifts in polyA site usage. **(B)** microRNA binding targets between the proximal and distal poly(A) sites of *Nphs1* and *Nphs2* mRNAs. In *Nphs1* mRNA, poly (A) site usage shifts to a distal site during injury, leading to a longer 3' UTR. This extended 3' UTR potentially alters post-transcriptional regulation by facilitating microRNA (miR) targeting (shown in red). These identified miRs include: miR-466d (binding score, 100), miR-376a-5p (score, 88) and miR-466c-5p (score, 76). In *Nphs2* mRNA, poly (A) site usage shifts to a proximal site during injury. This site is within exon 8, resulting in the loss of the canonical stop codon and potentially triggering non-stop decay. In addition, this shortened 3' UTR potentially alters post-transcriptional regulation by removing microRNA (miR) targeting (shown in red). These identified miRs include: miR-362-3p (score, 86) and miR-329-3p (score, 86), amongst others (not depicted) with varying scores. **(C)** Schematic showing the possible roles of alternatively splicing of *TJP1* and *ITM2B*

and alternative polyadenylation of *NEPH1*, *NPHS1* and *NPHS2* and in podocyte cytoskeleton and slit diaphragm regulation. In healthy podocytes, the core transmembrane components of slit diaphragm, NEPHRIN, PODOCIN, NEPH1, TJP1/ZO1 and ITM2B interact with each other and the actin cytoskeleton to maintain the structural and functional integrity of podocytes and the slit diaphragm. These healthy interactions involve relative proximal polyA site usage of *Neph1* and *Nphs1*, distal polyA site usage of *Nphs2*, and ↑*TJP1/ZO1* $\alpha+/\alpha-$ ratio and ↓*ITM2B S/L* ratios, which are reversed in injured podocytes due to alternative polyadenylation and alternative splicing. This is accompanied with decreased interactions with each other, and disruption of cytoskeleton and the slit diaphragm.

Table 1: Primers (5' to 3') used in the study

Gene/Isoform	Species	Forward	Reverse
***TJP1* (20+ and Δ)**	*Homo Sapiens*	CCTGGATTTAAGCCAGCCTC	CCCTGGGTGACTAACGGC
***TJP1* (20+ only)**	*Homo Sapiens*	CCTGGATTTAAGCCAGCCTC	GATGCTGGGTTTGTTTCAGGC
***TJP1* (20Δ only)**	*Homo Sapiens*	CCAACAGGTGTATAG	CCCTGGGTGACTAACGGC
***ITM2B* (Long only)**	*Homo Sapiens*	TGACGTTCAACTCCGCTCTG	AGTAGTACACGTCATCTGGTTGAA
***ITM2B* (Short only)**	*Homo Sapiens*	GAGCTTCCTCCACATTGGTC	AGTAGTACACGTCATCTGGTTGAA
RPL6	*Homo Sapiens*	GCAACCCTGTCCTTGTCAGA	GCCAGCTGCTTCAGGAAAAC
***Nphs1* (Internal)**	*Rattus Norvegicus*	TGCTCTTTGCAGTTGGTGGT	TCCTGATCCTGTCCTCCGAC
***Nphs2* (Internal)**	*Rattus Norvegicus*	ATTCCGACTGGGACATCTGC	TTCCAAGGTCTGGAGACGGA
***Neph1* (Internal)**	*Rattus Norvegicus*	TTGGTGCTCCCGACTTTGTT	CTCTGTCCATTGAGCCCCAG
***Gapdh* (Internal)**	*Rattus Norvegicus*	AAACCCATCACCATCTTCCA	GTGGTTCACACCCATCACAA
***Nphs1* (3'UTR)**	*Rattus Norvegicus*	GACACTGGATGTGGTTAGCG	GCATAAGCATGCACACATCGC
***Nphs2* (3'UTR)**	*Rattus Norvegicus*	AAAAGCTGCCTCTGAGTCCC	CTGTCACTGTCTTACACACC
***Neph1* (3' UTR)**	*Rattus Norvegicus*	ACAACCACTGGCCTTTGTGA	TAAAAGTGGAGGCAGCACGG
***Nphs1* (3' RACE)**	*Rattus Norvegicus*	GGATGTGGTTAGCGCAGAATG	*PolyA AUAP*
***Nphs2* (3' RACE)**	*Rattus Norvegicus*	GCCTCTGAGTCCCTGAGGATG	*PolyA AUAP*
***Neph1* (3' RACE)**	*Rattus Norvegicus*	ACAACCACTGGCCTTTGTGA	*PolyA AUAP*
***Gapdh* (3' RACE)**	*Rattus Norvegicus*	GCAAGAGAGAGGCCCTCAG	*PolyA AUAP*
PolyA Adapter			GGCCACGCGTCGACTAGTACTTTTTTTTTTTTTTTT
PolyA Abridged Universal Amplification Primer (AUAP)			GGCCACGCGTCGACTAGTAC

Table 2: Alternatively Spliced Genes

Table 2a: Monogenic Glomerular Disease Genes Represented in the Alternatively Spliced Genes in PAN and ADR Models			
Class	**Glomerulus**	**PAN (MCD)**	**ADR (FSGS)**
Podocytes	Membrane	*Podxl*	*Podxl*
	Cytoskeletal Scaffold	*Tns2, Inf2, Itsn2*	*Tns2, Inf2, Dlc1, Myh9*
	Lysosomal and endocytic		*Scarb2*
	Nucleoporins and transcription factors	*Lmna*	*Lmna*
	Slit Diaphragm	*Nphs1, Nphs2*	*Nphs1, Fat1*
	Metabolic and cystolic		*Ankfy1*
	Mitochondrial		*Coq2, Pdss2*
	Endothelial cells	*Inf2*	*Inf2*
Matrix	GBM	*Lamb2, Col4a4*	*Lamb2, Lama5, Col4a3, Col4a4, Col4a5*

Table 2b: Podocyte Genes Associated with Steroid Resistance Represented in the Alternatively Spliced Genes in PAN and ADR Models		
Class	**PAN (MCD)**	**ADR (FSGS)**
Actin Binding	*Inf2, Lamb2*	*Lamb2, Myh9, Myo1e, Inf2*
Slit membrane	*Nphs1, Nphs2*	*Fat1, Nphs1*
Lysosome		*Scarb2*
tRNA modification		*Cubn, Lage3*
Actin Regulation		*Kank2, Rac1, Dlc1, Cdc42*
CoQ biosynthesis		*Coq2, Pdss2*

Table 2c: Alternatively Spliced Genes with Established Roles in Glomerular Disease			
Gene		**PAN**	**ADR**
Coq2	CoenzymeQ2 / Polypolyprenyl transferase		3.77e-4
Pdss2	Decaprenyl Diphosphate Synthase Subunit 2		4.76e-3
Ankfy1	Ankyrin repeat and FYVE domain-containing protein 1		1.99e-4
Dlc1	Rho GTPase-activating protein 7		1.09e-4
Myh9	Myosin-9		5.05e-3
Tns2	Tenisn 2	2.73e-3	2.26e-4
Inf2	Inverted Formin 2	3.59e-3	3.45e-4
Itsn2	Intersectin 2	5.68e-3	
Podxl	Podocalyxin	6.76e-3	3.24e-4
Scarb2	Scavenger receptor class B member 2 or lysosomal integral membrane protein-2 (LIMP-2)		9.63e-3
Lmna	lamin A and C	5.59e-3	2.35e-3
Fat1	FAT1 cadherin protein		2.16e-4
Nphs1	Nephrin	9.62e-3	1.99e-4
Nphs2	Podocin	3.48e-3	
Myo1e	Myosin 1e		2.92e-4
Rac1	Rac Family Small GTPase 1		6.5e-3
Cdc42	Cell division control protein42		1.22e-3
Cubn	Cubilin		5.21e-3
Lage3	L antigen family member 3		4.63e-4
Col4a3	Collagen IV alpha 3		8.43e-5
Col4a4	Collagen IV alpha 4	1.71e-4	2.09e-4
Col4a5	Collagen IV alpha 5		9.37e-3
Lama5	Laminin-a5		5.73e-6
Lamb2	laminin-b2	2.88e-3	2.17e-3

Table 2d: Alternatively Spliced Genes with Novel Roles in Glomerular Disease			
Gene	**Protein**	**PAN**	**ADR**
Itm2b	Integral Transmembrane Protein 2B	1.05e-4	6.2e-26
Adgrg1	Adhesion G Protein-Coupled Receptor G1	---	5.01e-19
Polr1a	RNA Polymerase I Subunit A	---	3.96e-15
Tas1r2	Taste receptor type 1 member 2	---	6.42e-11
Tacc2	Transforming Acidic Coiled-Coil Containing Protein 2	4.32e-3	1.66e-10
Rgs3	Regulator Of G Protein Signaling 3	1.33e-7	7.18e-10
Cab39	Calcium Binding Protein 39	---	2.82e-3
Tjp1	Tight Junction Protein 1	1.38e-4	2.74e-3
Lima1	LIM Domain and Actin Binding 1	---	6.41e-9
Ampd2	Adenosine Monophosphate Deaminase 2	---	8.27e-9
Macf1	Microtubule-actin crosslinking factor 1	9.91e-5	1.79e-8
Cwc27	Spliceosome Associated Cyclophilin	---	2.34e-8

Table 3: Alternatively Polyadenylated Genes

Table 3a: Monogenic Glomerular Disease Genes Represented in the Alternatively Polyadenylated Genes in PAN and ADR Models			
Class	**Glomerulus**	**PAN (MCD)**	**ADR (FSGS)**
Podocytes	Membrane	*Podxl*	*Podxl*
	Cytoskeletal Scaffold	*Myh9*	*Myh9, Dlc1*
	Lysosomal and endocytic		*Scarb2*
	Nucleoporins and transcription factors	*Lmx1b*	*Wt1*
	Slit Diaphragm	*Kirrel1, Nphs1, Nphs2*	*Kirrel1, Nphs1, Nphs2*
	Endothelial cells		*Thbd*
Matrix	GBM	*Cd151*	*Cd151*

Table 3b: Podocyte Genes Associated with Steroid Resistance Represented in the Alternatively Polyadenylated Genes in PAN and ADR Models		
Class	**PAN (MCD)**	**ADR (FSGS)**
Actin Binding	*Myh9*	*Myh9*
Slit membrane	*Nphs1, Nphs2*	*Nphs1, Nphs2*
Lysosome		*Scarb2*
S1P metabolism		*Sgpl1*
Actin Regulation		*Rac1, Dlc1*

Table 3c: Alternative Polyadenylation Events in Genes with Known Roles in Glomerulopathy			
Genes	**Protein**	PAN (%)	ADR (%)
Podxl	Podocalyxin	50.45(P)	7.68 (P)
Myh9	Myosin-9	4.39 (D)	10.94 (D)
Dlc1	Rho GTPase-activating protein 7		13.41 (D)
Scarb2	Scavenger receptor class B member 2		19.95 (D)
Wt1	WT1 Transcription factor		10.31 (D)
Kirrel1	Kirre like nephrin family adhesion molecule 1	13.84 (D)	13.31 (D)
Nphs1	Nephrin, NPHS1 adhesion molecule	12.75 (D)	24.07 (D)
Nphs2	Podocin, NPHS2 stomatin family member	4.43 (P)	9.18 (P)
Cd151	CD151 molecule (Raph blood group), CD151 antigen	6.15 (D)	12.25 (D)
Thbd	Thrombomodulin		14.17 (D)
Lmx1b	LIM homeobox transcription factor 1 beta	10.18 (D)	
RAC1	Rac family small GTPase 1		5.86 (D)
SGPL1	sphingosine-1-phosphate lyase 1		17.66 (D)

Table 3d: Alternative Polyadenylation Events in Novel Genes			
Genes	**Protein**	PAN (%)	ADR (%)
Hsd17b14	hydroxysteroid (17-beta) dehydrogenase 14		45.38 (P)
Dph2	diphthamide biosynthesis 2		41.40 (D)
Dvl3	dishevelled segment polarity protein 3		40.63 (D)
Ccr5	C-C motif chemokine receptor 5		39.56 (D)
Foxn3	forkhead box N3	36.66 (D)	39.54 (D)
Ndrg2	NDRG family member 2		39.28 (D)
Slc25a24	solute carrier family 25 member 24		39.12 (D)
Nup50	nucleoporin 50		39.09 (D)
Cep43	centrosomal protein 43		38.88 (D)
Mgat3	beta-1,4-mannosyl-glycoprotein 4-beta-N-acetylglucosaminyltransferase		38.44 (D)

Supplementary Files:

Supplementary Figure S1

Serum chemistry of PAN- and adriamycin (ADR)- induced nephropathy animal models

Supplementary Figure S2

Ontology enrichment analyses of DEGs in PAN- and adriamycin (ADR)- induced nephropathy models

Supplementary Figure S3

DEGs in PAN and adriamycin (ADR) models deconvoluted for podocytes, other glomerular cells and parietal epithelial subtypes

Supplementary Figure S4

DEGs in PAN and adriamycin (ADR) models represented in established genes for glomerular disease and podocytopathies

Supplementary Figure S5

Dispersion plots depicted good fit for the PAN and adriamycin (ADR) models for exon/intron/junction analyses

Supplementary Figure S6

Heatmap of DEGs in the PAN and adriamycin (ADR) models represented in the dataset of a combination of transcription and translation machinery factors

Supplementary Figure S7

Manhattan plots depicting multi-population GWAS signals/SNPs localized in the regulatory regions of alternatively spliced genes and in the 3'UTR of alternatively polyadenylated genes in the PAN model

Supplementary Figure S8

Genomic organization of *Neph1, Nphs1 and Nphs2* genes and 3'UTR, Poly (A) site usage identified, RACE and 3'PCR primers used and sequence chromatograms obtained from RACE assays

Supplementary Table 1

Deconvolution of DEGs in PAN and adriamycin (ADR) models for parietal epithelial subtypes

Supplementary Table 2

Deconvolution of alternatively spliced genes in PAN and adriamycin (ADR) models for parietal epithelial subtypes

Supplementary Table 3

Alternatively spliced genes in PAN and adriamycin (ADR) models represented in monogenic genes with established roles in glomerular disease

Supplementary Table 4

Alternatively spliced genes in PAN and adriamycin (ADR) models representing novel genes in glomerular disease

Supplementary Table 5

Alternatively spliced genes reversed with pioglitazone treatment

Supplementary Table 6

Alternatively spliced genes reversed with GQ-16 treatment

Supplementary Table 7
Deconvolution of alternatively polyadenylated genes in PAN and adriamycin (ADR) models for parietal epithelial subtypes
Supplementary Table 8
Alternatively polyadenylated genes in PAN and adriamycin (ADR) models represented in monogenic genes with established roles in glomerular disease
Supplementary Table 9
Alternatively polyadenylated genes in PAN and adriamycin (ADR) models representing novel genes in glomerular disease
Supplementary Table 10
Alternatively polyadenylated genes reversed with pioglitazone treatment
Supplementary Table 11
Alternatively polyadenylated genes reversed with GQ-16 treatment
Supplementary Table 12
Dysregulated RBPs and splicing factors in PAN and adriamycin (ADR) models
Supplementary Table 13
Dysregulated pre-mRNA 3' processing and polyadenylation factors in PAN and adriamycin (ADR) models
Supplementary Table 14
Dysregulated transcription and translation machinery factors in PAN and adriamycin (ADR) models

References

1. Kerjaschki D. 2015 Homer W. Smith Award: The Podocyte from Periphery to Center Stage. Journal of the American Society of Nephrology : JASN. 2016;27(11):3266-70. Epub 2016/11/02. doi: 10.1681/ASN.2016040490. PubMed PMID: 27324941; PMCID: PMC5084903.
2. Siddall EC, Radhakrishnan J. The pathophysiology of edema formation in the nephrotic syndrome. Kidney Int. 2012;82(6):635-42. Epub 2012/06/22. doi: 10.1038/ki.2012.180. PubMed PMID: 22718186.
3. Radhakrishnan J. Hypercoagulopathy in nephrotic syndrome UpToDate2020. Available from: https://www.uptodate.com/contents/hypercoagulability-in-nephrotic-syndrome#H22.
4. Araya CE, Wasserfall CH, Brusko TM, Mu W, Segal MS, Johnson RJ, Garin EH. A case of unfulfilled expectations. Cytokines in idiopathic minimal lesion nephrotic syndrome. Pediatr Nephrol. 2006;21(5):603-10. Epub 2006/03/10. doi: 10.1007/s00467-006-0026-5. PubMed PMID: 16525836.
5. Araya C, Diaz L, Wasserfall C, Atkinson M, Mu W, Johnson R, Garin E. T regulatory cell function in idiopathic minimal lesion nephrotic syndrome. Pediatr Nephrol. 2009;24(9):1691-8. Epub 2009/06/06. doi: 10.1007/s00467-009-1214-x. PubMed PMID: 19495805; PMCID: PMC2785122.
6. Agrawal S, Zaritsky JJ, Fornoni A, Smoyer WE. Dyslipidaemia in nephrotic syndrome: mechanisms and treatment. Nat Rev Nephrol. 2018;14(1):57-70. Epub 2017/11/28. doi: 10.1038/nrneph.2017.155. PubMed PMID: 29176657; PMCID: PMC5770189.
7. Floege J, Barbour SJ, Cattran DC, Hogan JJ, Nachman PH, Tang SCW, Wetzels JFM, Cheung M, Wheeler DC, Winkelmayer WC, Rovin BH, Conference P. Management and treatment of glomerular diseases (part 1): conclusions from a Kidney Disease: Improving Global Outcomes (KDIGO) Controversies Conference. Kidney Int. 2019;95(2):268-80. Epub 2019/01/23. doi: 10.1016/j.kint.2018.10.018. PubMed PMID: 30665568.
8. Rovin BH, Caster DJ, Cattran DC, Gibson KL, Hogan JJ, Moeller MJ, Roccatello D, Cheung M, Wheeler DC, Winkelmayer WC, Floege J, Conference P. Management and treatment of glomerular diseases (part 2): conclusions from a Kidney Disease: Improving Global Outcomes (KDIGO) Controversies Conference. Kidney Int. 2019;95(2):281-95. Epub 2019/01/23. doi: 10.1016/j.kint.2018.11.008. PubMed PMID: 30665569.
9. Luyckx VA, Tonelli M, Stanifer JW. The global burden of kidney disease and the sustainable development goals. Bull World Health Organ. 2018;96(6):414-22D. Epub 2018/06/16. doi: 10.2471/BLT.17.206441. PubMed PMID: 29904224; PMCID: PMC5996218.
10. Valentini RP, Smoyer WE. Nephrotic Syndrome. In: Kher KW, Schnaper HW, Makker SP, editors. Clinical Pediatric Nephrology: Informa UK Ltd; 2007.
11. Hodson EM, Craig JC. Therapies for steroid-resistant nephrotic syndrome. Pediatr Nephrol. 2008;23(9):1391-4. Epub 2008/03/28. doi: 10.1007/s00467-008-0792-3. PubMed PMID: 18368428.
12. Longui CA. Glucocorticoid therapy: minimizing side effects. J Pediatr (Rio J). 2007;83(5 Suppl):S163-77. Epub 2007/11/15. doi: doi:10.2223/JPED.1713. PubMed PMID: 18000630.
13. Brosius J, Raabe CA. What is an RNA? A top layer for RNA classification. RNA Biol. 2016;13(2):140-4. Epub 2016/01/29. doi: 10.1080/15476286.2015.1128064. PubMed PMID: 26818079; PMCID: PMC4829331.
14. Li J, Liu C. Coding or Noncoding, the Converging Concepts of RNAs. Front Genet. 2019;10:496. Epub 2019/06/11. doi: 10.3389/fgene.2019.00496. PubMed PMID: 31178900; PMCID: PMC6538810.

15. Pan Q, Shai O, Lee LJ, Frey BJ, Blencowe BJ. Deep surveying of alternative splicing complexity in the human transcriptome by high-throughput sequencing. Nat Genet. 2008;40(12):1413-5. Epub 20081102. doi: 10.1038/ng.259. PubMed PMID: 18978789.
16. Scotti MM, Swanson MS. RNA mis-splicing in disease. Nature reviews Genetics. 2016;17(1):19-32. Epub 2015/11/26. doi: 10.1038/nrg.2015.3. PubMed PMID: 26593421; PMCID: PMC5993438.
17. Blijlevens M, Li J, van Beusechem VW. Biology of the mRNA Splicing Machinery and Its Dysregulation in Cancer Providing Therapeutic Opportunities. Int J Mol Sci. 2021;22(10). Epub 2021/06/03. doi: 10.3390/ijms22105110. PubMed PMID: 34065983; PMCID: PMC8150589.
18. Montes M, Sanford BL, Comiskey DF, Chandler DS. RNA Splicing and Disease: Animal Models to Therapies. Trends Genet. 2019;35(1):68-87. Epub 2018/11/24. doi: 10.1016/j.tig.2018.10.002. PubMed PMID: 30466729; PMCID: PMC6339821.
19. Agrawal S, Eng C. Differential expression of novel naturally occurring splice variants of PTEN and their functional consequences in Cowden syndrome and sporadic breast cancer. Human molecular genetics. 2006;15(5):777-87. Epub 2006/01/27. doi: 10.1093/hmg/ddi492. PubMed PMID: 16436456.
20. Agrawal S, Pilarski R, Eng C. Different splicing defects lead to differential effects downstream of the lipid and protein phosphatase activities of PTEN. Human molecular genetics. 2005;14(16):2459-68. Epub 2005/07/15. doi: 10.1093/hmg/ddi246. PubMed PMID: 16014636.
21. Plon SE, Pirics ML, Nuchtern J, Hicks J, Russell H, Agrawal S, Zbuk K, Eng C, Hegde M, Chin EL. Multiple tumors in a child with germ-line mutations in TP53 and PTEN. The New England journal of medicine. 2008;359(5):537-9. Epub 2008/08/02. doi: 10.1056/NEJMc0800627. PubMed PMID: 18669439.
22. Sarquis MS, Agrawal S, Shen L, Pilarski R, Zhou XP, Eng C. Distinct expression profiles for PTEN transcript and its splice variants in Cowden syndrome and Bannayan-Riley-Ruvalcaba syndrome. American journal of human genetics. 2006;79(1):23-30. Epub 2006/06/15. doi: 10.1086/504392. PubMed PMID: 16773562; PMCID: 1474112.
23. Stevens M, Oltean S. Alternative Splicing in CKD. Journal of the American Society of Nephrology : JASN. 2016;27(6):1596-603. Epub 2016/01/15. doi: 10.1681/ASN.2015080908. PubMed PMID: 26763787; PMCID: PMC4884122.
24. Bryant C, Webb A, Banks AS, Chandler D, Govindarajan R, Agrawal S. Alternatively Spliced Landscape of PPARgamma mRNA in Podocytes Is Distinct from Adipose Tissue. Cells. 2022;11(21). Epub 20221101. doi: 10.3390/cells11213455. PubMed PMID: 36359851.
25. Derti A, Garrett-Engele P, Macisaac KD, Stevens RC, Sriram S, Chen R, Rohl CA, Johnson JM, Babak T. A quantitative atlas of polyadenylation in five mammals. Genome Res. 2012;22(6):1173-83. Epub 2012/03/29. doi: 10.1101/gr.132563.111. PubMed PMID: 22454233; PMCID: PMC3371698.
26. Brumbaugh J, Di Stefano B, Wang X, Borkent M, Forouzmand E, Clowers KJ, Ji F, Schwarz BA, Kalocsay M, Elledge SJ, Chen Y, Sadreyev RI, Gygi SP, Hu G, Shi Y, Hochedlinger K. Nudt21 Controls Cell Fate by Connecting Alternative Polyadenylation to Chromatin Signaling. Cell. 2018;172(3):629-31. Epub 2018/01/27. doi: 10.1016/j.cell.2017.12.035. PubMed PMID: 29373832; PMCID: PMC5831378.
27. Sandberg R, Neilson JR, Sarma A, Sharp PA, Burge CB. Proliferating cells express mRNAs with shortened 3' untranslated regions and fewer microRNA target sites. Science. 2008;320(5883):1643-7. Epub 2008/06/21. doi: 10.1126/science.1155390. PubMed PMID: 18566288; PMCID: PMC2587246.

28. Alt FW, Bothwell AL, Knapp M, Siden E, Mather E, Koshland M, Baltimore D. Synthesis of secreted and membrane-bound immunoglobulin mu heavy chains is directed by mRNAs that differ at their 3' ends. Cell. 1980;20(2):293-301. Epub 1980/06/01. doi: 10.1016/0092-8674(80)90615-7. PubMed PMID: 6771018.
29. Ji Z, Lee JY, Pan Z, Jiang B, Tian B. Progressive lengthening of 3' untranslated regions of mRNAs by alternative polyadenylation during mouse embryonic development. Proceedings of the National Academy of Sciences of the United States of America. 2009;106(17):7028-33. Epub 2009/04/18. doi: 10.1073/pnas.0900028106. PubMed PMID: 19372383; PMCID: PMC2669788.
30. Lee SH, Singh I, Tisdale S, Abdel-Wahab O, Leslie CS, Mayr C. Widespread intronic polyadenylation inactivates tumour suppressor genes in leukaemia. Nature. 2018;561(7721):127-31. Epub 2018/08/29. doi: 10.1038/s41586-018-0465-8. PubMed PMID: 30150773; PMCID: PMC6527314.
31. Singh I, Lee SH, Sperling AS, Samur MK, Tai YT, Fulciniti M, Munshi NC, Mayr C, Leslie CS. Widespread intronic polyadenylation diversifies immune cell transcriptomes. Nat Commun. 2018;9(1):1716. Epub 2018/05/02. doi: 10.1038/s41467-018-04112-z. PubMed PMID: 29712909; PMCID: PMC5928244.
32. Mayr C, Bartel DP. Widespread shortening of 3'UTRs by alternative cleavage and polyadenylation activates oncogenes in cancer cells. Cell. 2009;138(4):673-84. Epub 2009/08/26. doi: 10.1016/j.cell.2009.06.016. PubMed PMID: 19703394; PMCID: PMC2819821.
33. Masamha CP, Xia Z, Yang J, Albrecht TR, Li M, Shyu AB, Li W, Wagner EJ. CFIm25 links alternative polyadenylation to glioblastoma tumour suppression. Nature. 2014;510(7505):412-6. Epub 2014/05/13. doi: 10.1038/nature13261. PubMed PMID: 24814343; PMCID: PMC4128630.
34. Mueller AA, van Velthoven CT, Fukumoto KD, Cheung TH, Rando TA. Intronic polyadenylation of PDGFRalpha in resident stem cells attenuates muscle fibrosis. Nature. 2016;540(7632):276-9. Epub 2016/11/29. doi: 10.1038/nature20160. PubMed PMID: 27894125; PMCID: PMC5384334.
35. Hoque M, Ji Z, Zheng D, Luo W, Li W, You B, Park JY, Yehia G, Tian B. Analysis of alternative cleavage and polyadenylation by 3' region extraction and deep sequencing. Nat Methods. 2013;10(2):133-9. Epub 20121216. doi: 10.1038/nmeth.2288. PubMed PMID: 23241633; PMCID: PMC3560312.
36. Hartley SW, Mullikin JC. Detection and visualization of differential splicing in RNA-Seq data with JunctionSeq. Nucleic acids research. 2016;44(15):e127. Epub 20160601. doi: 10.1093/nar/gkw501. PubMed PMID: 27257077; PMCID: PMC5009739.
37. Wang Y, Xie Z, Kutschera E, Adams JI, Kadash-Edmondson KE, Xing Y. rMATS-turbo: an efficient and flexible computational tool for alternative splicing analysis of large-scale RNA-seq data. Nat Protoc. 2024;19(4):1083-104. Epub 20240223. doi: 10.1038/s41596-023-00944-2. PubMed PMID: 38396040.
38. Ye C, Long Y, Ji G, Li QQ, Wu X. APAtrap: identification and quantification of alternative polyadenylation sites from RNA-seq data. Bioinformatics. 2018;34(11):1841-9. Epub 2018/01/24. doi: 10.1093/bioinformatics/bty029. PubMed PMID: 29360928.
39. Bryant C, Rask G, Waller AP, Webb A, Galdino-Pitta MR, Amato AA, Cianciolo R, Govindarajan R, Becknell B, Kerlin BA, Neves FAR, Fornoni A, Agrawal S. Selective modulator of nuclear receptor PPARgamma with reduced adipogenic potential ameliorates experimental nephrotic syndrome. iScience. 2022;25(4):104001. Epub 2022/03/22. doi: 10.1016/j.isci.2022.104001. PubMed PMID: 35310946; PMCID: PMC8927998.
40. Rinschen MM, Godel M, Grahammer F, Zschiedrich S, Helmstadter M, Kretz O, Zarei M, Braun DA, Dittrich S, Pahmeyer C, Schroder P, Teetzen C, Gee H, Daouk G, Pohl M, Kuhn E, Schermer B, Kuttner V, Boerries M, Busch H, Schiffer M, Bergmann C, Kruger M, Hildebrandt F, Dengjel

J, Benzing T, Huber TB. A Multi-layered Quantitative In Vivo Expression Atlas of the Podocyte Unravels Kidney Disease Candidate Genes. Cell reports. 2018;23(8):2495-508. doi: 10.1016/j.celrep.2018.04.059. PubMed PMID: 29791858; PMCID: PMC5986710.

41. Karaiskos N, Rahmatollahi M, Boltengagen A, Liu H, Hoehne M, Rinschen M, Schermer B, Benzing T, Rajewsky N, Kocks C, Kann M, Muller RU. A Single-Cell Transcriptome Atlas of the Mouse Glomerulus. Journal of the American Society of Nephrology : JASN. 2018;29(8):2060-8. Epub 20180524. doi: 10.1681/ASN.2018030238. PubMed PMID: 29794128; PMCID: PMC6065081.
42. Liu WB, Huang GR, Liu BL, Hu HK, Geng J, Rui HL, Gao C, Huang YJ, Huo GY, Mao JR, Lu CJ, Xu AL. Single cell landscape of parietal epithelial cells in healthy and diseased states. Kidney Int. 2023;104(1):108-23. Epub 20230424. doi: 10.1016/j.kint.2023.03.036. PubMed PMID: 37100348.
43. Li AS, Ingham JF, Lennon R. Genetic Disorders of the Glomerular Filtration Barrier. Clin J Am Soc Nephrol. 2020;15(12):1818-28. Epub 2020/03/25. doi: 10.2215/CJN.11440919. PubMed PMID: 32205319; PMCID: PMC7769017.
44. Kopp JB, Anders HJ, Susztak K, Podesta MA, Remuzzi G, Hildebrandt F, Romagnani P. Podocytopathies. Nat Rev Dis Primers. 2020;6(1):68. Epub 20200813. doi: 10.1038/s41572-020-0196-7. PubMed PMID: 32792490; PMCID: PMC8162925.
45. Chen M, Manley JL. Mechanisms of alternative splicing regulation: insights from molecular and genomics approaches. Nat Rev Mol Cell Biol. 2009;10(11):741-54. Epub 2009/09/24. doi: 10.1038/nrm2777. PubMed PMID: 19773805; PMCID: PMC2958924.
46. Rogalska ME, Vivori C, Valcarcel J. Regulation of pre-mRNA splicing: roles in physiology and disease, and therapeutic prospects. Nature reviews Genetics. 2023;24(4):251-69. Epub 20221216. doi: 10.1038/s41576-022-00556-8. PubMed PMID: 36526860.
47. Tian B, Manley JL. Alternative polyadenylation of mRNA precursors. Nat Rev Mol Cell Biol. 2017;18(1):18-30. Epub 2016/11/04. doi: 10.1038/nrm.2016.116. PubMed PMID: 27677860; PMCID: PMC5483950.
48. Shi Y, Di Giammartino DC, Taylor D, Sarkeshik A, Rice WJ, Yates JR, 3rd, Frank J, Manley JL. Molecular architecture of the human pre-mRNA 3' processing complex. Mol Cell. 2009;33(3):365-76. doi: 10.1016/j.molcel.2008.12.028. PubMed PMID: 19217410; PMCID: PMC2946185.
49. Mitschka S, Mayr C. Context-specific regulation and function of mRNA alternative polyadenylation. Nat Rev Mol Cell Biol. 2022;23(12):779-96. Epub 20220707. doi: 10.1038/s41580-022-00507-5. PubMed PMID: 35798852; PMCID: PMC9261900.
50. Barry A, McNulty MT, Jia X, Gupta Y, Debiec H, Luo Y, Nagano C, Horinouchi T, Jung S, Colucci M, Ahram DF, Mitrotti A, Sinha A, Teeninga N, Jin G, Shril S, Caridi G, Bodria M, Lim TY, Westland R, Zanoni F, Marasa M, Turudic D, Giordano M, Gesualdo L, Magistroni R, Pisani I, Fiaccadori E, Reiterova J, Maringhini S, Morello W, Montini G, Weng PL, Scolari F, Saraga M, Tasic V, Santoro D, van Wijk JAE, Milosevic D, Kawai Y, Kiryluk K, Pollak MR, Gharavi A, Lin F, Simoes ESAC, Loos RJF, Kenny EE, Schreuder MF, Zurowska A, Dossier C, Ariceta G, Drozynska-Duklas M, Hogan J, Jankauskiene A, Hildebrandt F, Prikhodina L, Song K, Bagga A, Cheong H, 2nd, Ghiggeri GM, Vachvanichsanong P, Nozu K, Lee D, Vivarelli M, Raychaudhuri S, Tokunaga K, Sanna-Cherchi S, Ronco P, Iijima K, Sampson MG. Multi-population genome-wide association study implicates immune and non-immune factors in pediatric steroid-sensitive nephrotic syndrome. Nat Commun. 2023;14(1):2481. Epub 20230429. doi: 10.1038/s41467-023-37985-w. PubMed PMID: 37120605; PMCID: PMC10148875.

51. Kocylowski MK, Aypek H, Bildl W, Helmstadter M, Trachte P, Dumoulin B, Wittosch S, Kuhne L, Aukschun U, Teetzen C, Kretz O, Gaal B, Kulik A, Antignac C, Mollet G, Kottgen A, Gocmen B, Schwenk J, Schulte U, Huber TB, Fakler B, Grahammer F. A slit-diaphragm-associated protein network for dynamic control of renal filtration. Nat Commun. 2022;13(1):6446. Epub 20221028. doi: 10.1038/s41467-022-33748-1. PubMed PMID: 36307401; PMCID: PMC9616960.
52. Grahammer F, Schell C, Huber TB. The podocyte slit diaphragm--from a thin grey line to a complex signalling hub. Nat Rev Nephrol. 2013;9(10):587-98. Epub 2013/09/04. doi: 10.1038/nrneph.2013.169. PubMed PMID: 23999399.
53. Grahammer F, Wigge C, Schell C, Kretz O, Patrakka J, Schneider S, Klose M, Kind J, Arnold SJ, Habermann A, Brauniger R, Rinschen MM, Volker L, Bregenzer A, Rubbenstroth D, Boerries M, Kerjaschki D, Miner JH, Walz G, Benzing T, Fornoni A, Frangakis AS, Huber TB. A flexible, multilayered protein scaffold maintains the slit in between glomerular podocytes. JCI Insight. 2016;1(9). Epub 2016/07/19. doi: 10.1172/jci.insight.86177. PubMed PMID: 27430022; PMCID: PMC4943462.
54. Grahammer F, Benzing T, Huber TB. New insights into mechanisms of glomerular injury and repair from the 10th International Podocyte Conference 2014. Kidney Int. 2015;87(5):885-93. Epub 2015/02/26. doi: 10.1038/ki.2015.5. PubMed PMID: 25715118.
55. Schnabel E, Anderson JM, Farquhar MG. The tight junction protein ZO-1 is concentrated along slit diaphragms of the glomerular epithelium. The Journal of cell biology. 1990;111(3):1255-63. doi: 10.1083/jcb.111.3.1255. PubMed PMID: 2202736; PMCID: PMC2116287.
56. Fukasawa H, Bornheimer S, Kudlicka K, Farquhar MG. Slit diaphragms contain tight junction proteins. Journal of the American Society of Nephrology : JASN. 2009;20(7):1491-503. Epub 20090528. doi: 10.1681/ASN.2008101117. PubMed PMID: 19478094; PMCID: PMC2709684.
57. Shono A, Tsukaguchi H, Yaoita E, Nameta M, Kurihara H, Qin XS, Yamamoto T, Doi T. Podocin participates in the assembly of tight junctions between foot processes in nephrotic podocytes. Journal of the American Society of Nephrology : JASN. 2007;18(9):2525-33. Epub 20070805. doi: 10.1681/ASN.2006101084. PubMed PMID: 17675666.
58. Choi SI, Vidal R, Frangione B, Levy E. Axonal transport of British and Danish amyloid peptides via secretory vesicles. FASEB journal : official publication of the Federation of American Societies for Experimental Biology. 2004;18(2):373-5. Epub 20031204. doi: 10.1096/fj.03-0730fje. PubMed PMID: 14656991.
59. Damase TR, Sukhovershin R, Boada C, Taraballi F, Pettigrew RI, Cooke JP. The Limitless Future of RNA Therapeutics. Front Bioeng Biotechnol. 2021;9:628137. Epub 2021/04/06. doi: 10.3389/fbioe.2021.628137. PubMed PMID: 33816449; PMCID: PMC8012680.
60. Paunovska K, Loughrey D, Dahlman JE. Drug delivery systems for RNA therapeutics. Nature reviews Genetics. 2022. Epub 2022/01/06. doi: 10.1038/s41576-021-00439-4. PubMed PMID: 34983972; PMCID: PMC8724758.
61. Lieberman J. Tapping the RNA world for therapeutics. Nature structural & molecular biology. 2018;25(5):357-64. Epub 2018/04/18. doi: 10.1038/s41594-018-0054-4. PubMed PMID: 29662218; PMCID: PMC6052442.
62. Seufert L, Benzing T, Ignarski M, Muller RU. RNA-binding proteins and their role in kidney disease. Nat Rev Nephrol. 2021. Epub 2021/11/05. doi: 10.1038/s41581-021-00497-1. PubMed PMID: 34732838.
63. Wu H, Gonzalez Villalobos R, Yao X, Reilly D, Chen T, Rankin M, Myshkin E, Breyer MD, Humphreys BD. Mapping the single-cell transcriptomic response of murine diabetic kidney disease to therapies. Cell metabolism. 2022;34(7):1064-78 e6. Epub 20220615. doi: 10.1016/j.cmet.2022.05.010. PubMed PMID: 35709763; PMCID: PMC9262852.

64. Wineberg Y, Bar-Lev TH, Futorian A, Ben-Haim N, Armon L, Ickowicz D, Oriel S, Bucris E, Yehuda Y, Pode-Shakked N, Gilad S, Benjamin S, Hohenstein P, Dekel B, Urbach A, Kalisky T. Single-Cell RNA Sequencing Reveals mRNA Splice Isoform Switching during Kidney Development. Journal of the American Society of Nephrology : JASN. 2020;31(10):2278-91. Epub 20200710. doi: 10.1681/ASN.2019080770. PubMed PMID: 32651222; PMCID: PMC7609002.
65. Vivarelli M, Massella L, Ruggiero B, Emma F. Minimal Change Disease. Clin J Am Soc Nephrol. 2017;12(2):332-45. Epub 20161209. doi: 10.2215/CJN.05000516. PubMed PMID: 27940460; PMCID: PMC5293332.
66. Shabaka A, Tato Ribera A, Fernandez-Juarez G. Focal Segmental Glomerulosclerosis: State-of-the-Art and Clinical Perspective. Nephron. 2020;144(9):413-27. Epub 20200728. doi: 10.1159/000508099. PubMed PMID: 32721952.
67. Maas RJ, Deegens JK, Smeets B, Moeller MJ, Wetzels JF. Minimal change disease and idiopathic FSGS: manifestations of the same disease. Nat Rev Nephrol. 2016;12(12):768-76. Epub 20161017. doi: 10.1038/nrneph.2016.147. PubMed PMID: 27748392.
68. Agrawal S, Guess AJ, Benndorf R, Smoyer WE. Comparison of direct action of thiazolidinediones and glucocorticoids on renal podocytes: protection from injury and molecular effects. Molecular pharmacology. 2011;80(3):389-99. Epub 2011/06/04. doi: 10.1124/mol.111.071654. PubMed PMID: 21636793; PMCID: 3164328.
69. Agrawal S, Chanley MA, Westbrook D, Nie X, Kitao T, Guess AJ, Benndorf R, Hidalgo G, Smoyer WE. Pioglitazone Enhances the Beneficial Effects of Glucocorticoids in Experimental Nephrotic Syndrome. Sci Rep. 2016;6:24392. Epub 2016/05/05. doi: 10.1038/srep24392. PubMed PMID: 27142691; PMCID: 4855145.
70. Itoh M, Nakadate K, Horibata Y, Matsusaka T, Xu J, Hunziker W, Sugimoto H. The structural and functional organization of the podocyte filtration slits is regulated by Tjp1/ZO-1. PloS one. 2014;9(9):e106621. Epub 2014/09/04. doi: 10.1371/journal.pone.0106621. PubMed PMID: 25184792; PMCID: PMC4153657.
71. Willott E, Balda MS, Heintzelman M, Jameson B, Anderson JM. Localization and differential expression of two isoforms of the tight junction protein ZO-1. The American journal of physiology. 1992;262(5 Pt 1):C1119-24. doi: 10.1152/ajpcell.1992.262.5.C1119. PubMed PMID: 1590354.
72. Balda MS, Anderson JM. Two classes of tight junctions are revealed by ZO-1 isoforms. The American journal of physiology. 1993;264(4 Pt 1):C918-24. Epub 1993/04/01. doi: 10.1152/ajpcell.1993.264.4.C918. PubMed PMID: 7682777.
73. Kim YE, Won M, Lee SG, Park C, Song CH, Kim KK. RBM47-regulated alternative splicing of TJP1 promotes actin stress fiber assembly during epithelial-to-mesenchymal transition. Oncogene. 2019;38(38):6521-36. Epub 2019/07/31. doi: 10.1038/s41388-019-0892-5. PubMed PMID: 31358901.
74. Wohlschlegel J, Argentini M, Michiels C, Letellier C, Forster V, Condroyer C, He Z, Thuret G, Zeitz C, Leger T, Audo I. First identification of ITM2B interactome in the human retina. Sci Rep. 2021;11(1):17210. Epub 20210826. doi: 10.1038/s41598-021-96571-6. PubMed PMID: 34446781; PMCID: PMC8390696.
75. Gallicchio L, Olivares GH, Berry CW, Fuller MT. Regulation and function of alternative polyadenylation in development and differentiation. RNA Biol. 2023;20(1):908-25. Epub 20231031. doi: 10.1080/15476286.2023.2275109. PubMed PMID: 37906624; PMCID: PMC10730144.

76. Mohanan NK, Shaji F, Koshre GR, Laishram RS. Alternative polyadenylation: An enigma of transcript length variation in health and disease. Wiley Interdiscip Rev RNA. 2022;13(1):e1692. Epub 20210927. doi: 10.1002/wrna.1692. PubMed PMID: 34581021.
77. Mukherjee S, Graber JH, Moore CL. Macrophage differentiation is marked by increased abundance of the mRNA 3' end processing machinery, altered poly(A) site usage, and sensitivity to the level of CstF64. Front Immunol. 2023;14:1091403. Epub 20230125. doi: 10.3389/fimmu.2023.1091403. PubMed PMID: 36761770; PMCID: PMC9905730.
78. Egli M, Manoharan M. Chemistry, structure and function of approved oligonucleotide therapeutics. Nucleic acids research. 2023;51(6):2529-73. doi: 10.1093/nar/gkad067. PubMed PMID: 36881759; PMCID: PMC10085713.
79. Douglas AG, Wood MJ. Splicing therapy for neuromuscular disease. Mol Cell Neurosci. 2013;56:169-85. Epub 2013/05/02. doi: 10.1016/j.mcn.2013.04.005. PubMed PMID: 23631896; PMCID: PMC3793868.
80. Pippin JW, Brinkkoetter PT, Cormack-Aboud FC, Durvasula RV, Hauser PV, Kowalewska J, Krofft RD, Logar CM, Marshall CB, Ohse T, Shankland SJ. Inducible rodent models of acquired podocyte diseases. American journal of physiology Renal physiology. 2009;296(2):F213-29. Epub 2008/09/12. doi: 10.1152/ajprenal.90421.2008. PubMed PMID: 18784259.
81. Barbosa-Morais NL, Irimia M, Pan Q, Xiong HY, Gueroussov S, Lee LJ, Slobodeniuc V, Kutter C, Watt S, Colak R, Kim T, Misquitta-Ali CM, Wilson MD, Kim PM, Odom DT, Frey BJ, Blencowe BJ. The evolutionary landscape of alternative splicing in vertebrate species. Science. 2012;338(6114):1587-93. doi: 10.1126/science.1230612. PubMed PMID: 23258890.
82. Wang R, Zheng D, Yehia G, Tian B. A compendium of conserved cleavage and polyadenylation events in mammalian genes. Genome Res. 2018;28(10):1427-41. Epub 20180824. doi: 10.1101/gr.237826.118. PubMed PMID: 30143597; PMCID: PMC6169888.
83. Ara T, Lopez F, Ritchie W, Benech P, Gautheret D. Conservation of alternative polyadenylation patterns in mammalian genes. BMC Genomics. 2006;7:189. Epub 20060726. doi: 10.1186/1471-2164-7-189. PubMed PMID: 16872498; PMCID: PMC1550727.
84. Luimula P, Aaltonen P, Ahola H, Palmen T, Holthofer H. Alternatively spliced nephrin in experimental glomerular disease of the rat. Pediatr Res. 2000;48(6):759-62. doi: 10.1203/00006450-200012000-00010. PubMed PMID: 11102543.
85. Holthofer H, Ahola H, Solin ML, Wang S, Palmen T, Luimula P, Miettinen A, Kerjaschki D. Nephrin localizes at the podocyte filtration slit area and is characteristically spliced in the human kidney. Am J Pathol. 1999;155(5):1681-7. doi: 10.1016/S0002-9440(10)65483-1. PubMed PMID: 10550324; PMCID: PMC1866978.
86. Relle M, Cash H, Brochhausen C, Strand D, Menke J, Galle PR, Schwarting A. New perspectives on the renal slit diaphragm protein podocin. Mod Pathol. 2011;24(8):1101-10. Epub 20110415. doi: 10.1038/modpathol.2011.58. PubMed PMID: 21499232; PMCID: PMC3182839.
87. Fu T, Chan TW, Bahn JH, Kim TH, Rowat AC, Xiao X. Multifaceted role of RNA editing in promoting loss-of-function of PODXL in cancer. iScience. 2022;25(8):104836. Epub 20220802. doi: 10.1016/j.isci.2022.104836. PubMed PMID: 35992085; PMCID: PMC9382340.
88. Chen L. Two Tales of Single-Cell RNA Sequencing: Gene Expression and Alternative Splicing in Mouse Kidney Development. Journal of the American Society of Nephrology : JASN. 2020;31(10):2234-6. Epub 20200903. doi: 10.1681/ASN.2020081180. PubMed PMID: 32883701; PMCID: PMC7608996.
89. Belchikov N, Hsu J, Li XJ, Jarroux J, Hu W, Joglekar A, Tilgner HU. Understanding isoform expression by pairing long-read sequencing with single-cell and spatial transcriptomics. Genome

Res. 2024;34(11):1735-46. Epub 20241120. doi: 10.1101/gr.279640.124. PubMed PMID: 39567235; PMCID: PMC11610585.

90. Gao Y, Li L, Amos CI, Li W. Analysis of alternative polyadenylation from single-cell RNA-seq using scDaPars reveals cell subpopulations invisible to gene expression. Genome Res. 2021;31(10):1856-66. Epub 20210525. doi: 10.1101/gr.271346.120. PubMed PMID: 34035046; PMCID: PMC8494218.
91. Tian B. Decoding the end of message: PASTA provides food for thought on mechanisms of alternative polyadenylation. Mol Cell. 2024;84(15):2804-6. doi: 10.1016/j.molcel.2024.07.015. PubMed PMID: 39121842.

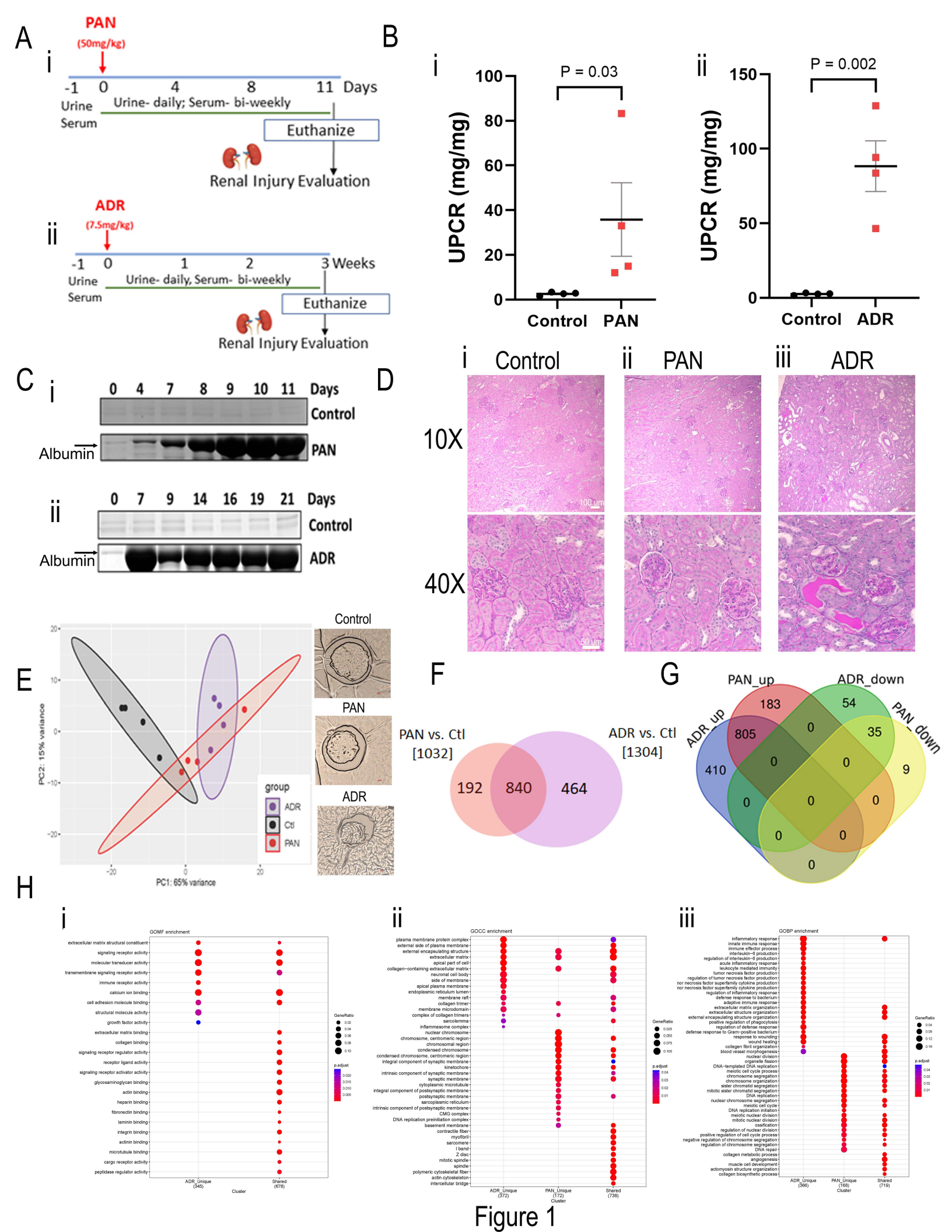
A
i
PAN
(50mg/kg)
-1 0 4 8 11 Days
Urine
Serum
Urine- daily; Serum- bi-weekly
Euthanize
Renal Injury Evaluation
ii
ADR
(7.5mg/kg)
-1 0 1 2 3 Weeks
Urine
Serum
Urine- daily, Serum- bi-weekly
Euthanize
Renal Injury Evaluation
B
i
P = 0.03
UPCR (mg/mg)
Control
PAN
ii
P = 0.002
UPCR (mg/mg)
Control
ADR
C
i
0 4 7 8 9 10 11 Days
Control
Albumin
PAN
ii
0 7 9 14 16 19 21 Days
Control
Albumin
ADR
D
i Control
ii PAN
iii ADR
10X
40X
E
PC2: 15% variance
PC1: 65% variance
group
ADR
Ctl
PAN
Control
PAN
ADR
F
PAN vs. Ctl
[1032]
192
840
464
ADR vs. Ctl
[1304]
G
PAN_up
ADR_down
ADR_up
PAN_down
183
54
805
35
410
9
0
H
i
GOMF enrichment
Cluster
ADR_Unique (345)
Shared (676)
ii
GOCC enrichment
Cluster
ADR_Unique (372)
PAN_Unique (172)
Shared (738)
iii
GOBP enrichment
Cluster
ADR_Unique (366)
PAN_Unique (168)
Shared (719)

Figure 1

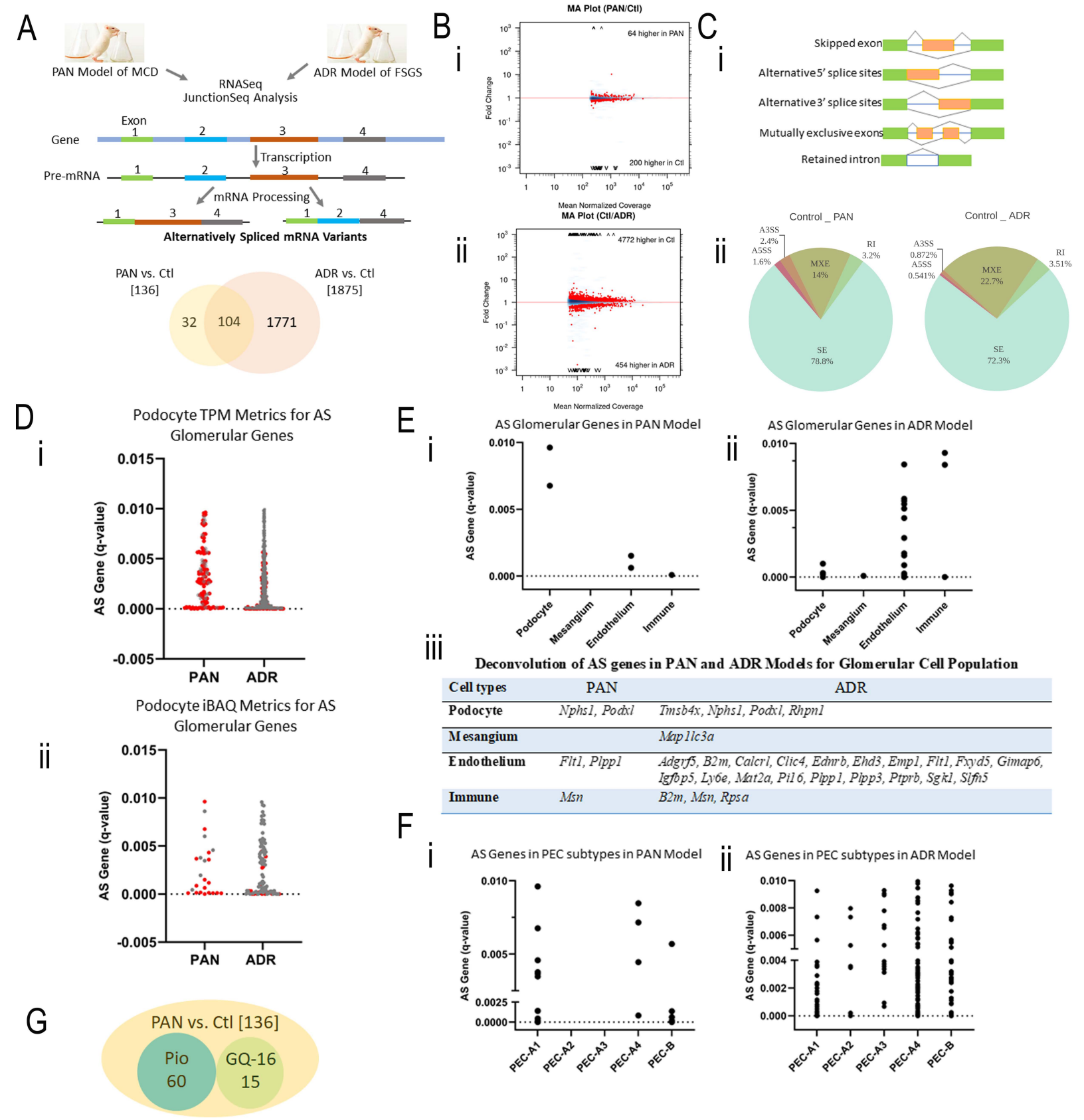
A
PAN Model of MCD
ADR Model of FSGS
RNASeq
JunctionSeq Analysis
Exon
Gene
Transcription
Pre-mRNA
mRNA Processing
Alternatively Spliced mRNA Variants
PAN vs. Ctl
[136]
ADR vs. Ctl
[1875]
32
104
1771
B
i
MA Plot (PAN/Ctl)
64 higher in PAN
200 higher in Ctl
Fold Change
Mean Normalized Coverage
ii
MA Plot (Ctl/ADR)
4772 higher in Ctl
454 higher in ADR
C
i
Skipped exon
Alternative 5' splice sites
Alternative 3' splice sites
Mutually exclusive exons
Retained intron
ii
Control _ PAN
Control _ ADR
A3SS
A5SS
RI
MXE
SE
D
i
Podocyte TPM Metrics for AS Glomerular Genes
AS Gene (q-value)
PAN
ADR
ii
Podocyte iBAQ Metrics for AS Glomerular Genes
E
i
AS Glomerular Genes in PAN Model
ii
AS Glomerular Genes in ADR Model
Podocyte
Mesangium
Endothelium
Immune
iii
Deconvolution of AS genes in PAN and ADR Models for Glomerular Cell Population
Cell types | PAN | ADR
Podocyte | Nphs1, Podxl | Tmsb4x, Nphs1, Podxl, Rhpn1
Mesangium | | Map1lc3a
Endothelium | Flt1, Plpp1 | Adgrf5, B2m, Calcrl, Clic4, Ednrb, Ehd3, Emp1, Flt1, Fxyd5, Gimap6, Igfbp5, Ly6e, Mat2a, Pil6, Plpp1, Plpp3, Ptprb, Sgk1, Slfn5
Immune | Msn | B2m, Msn, Rpsa
F
i
AS Genes in PEC subtypes in PAN Model
ii
AS Genes in PEC subtypes in ADR Model
PEC-A1
PEC-A2
PEC-A3
PEC-A4
PEC-B
G
PAN vs. Ctl [136]
Pio
60
GQ-16
15

Figure 2

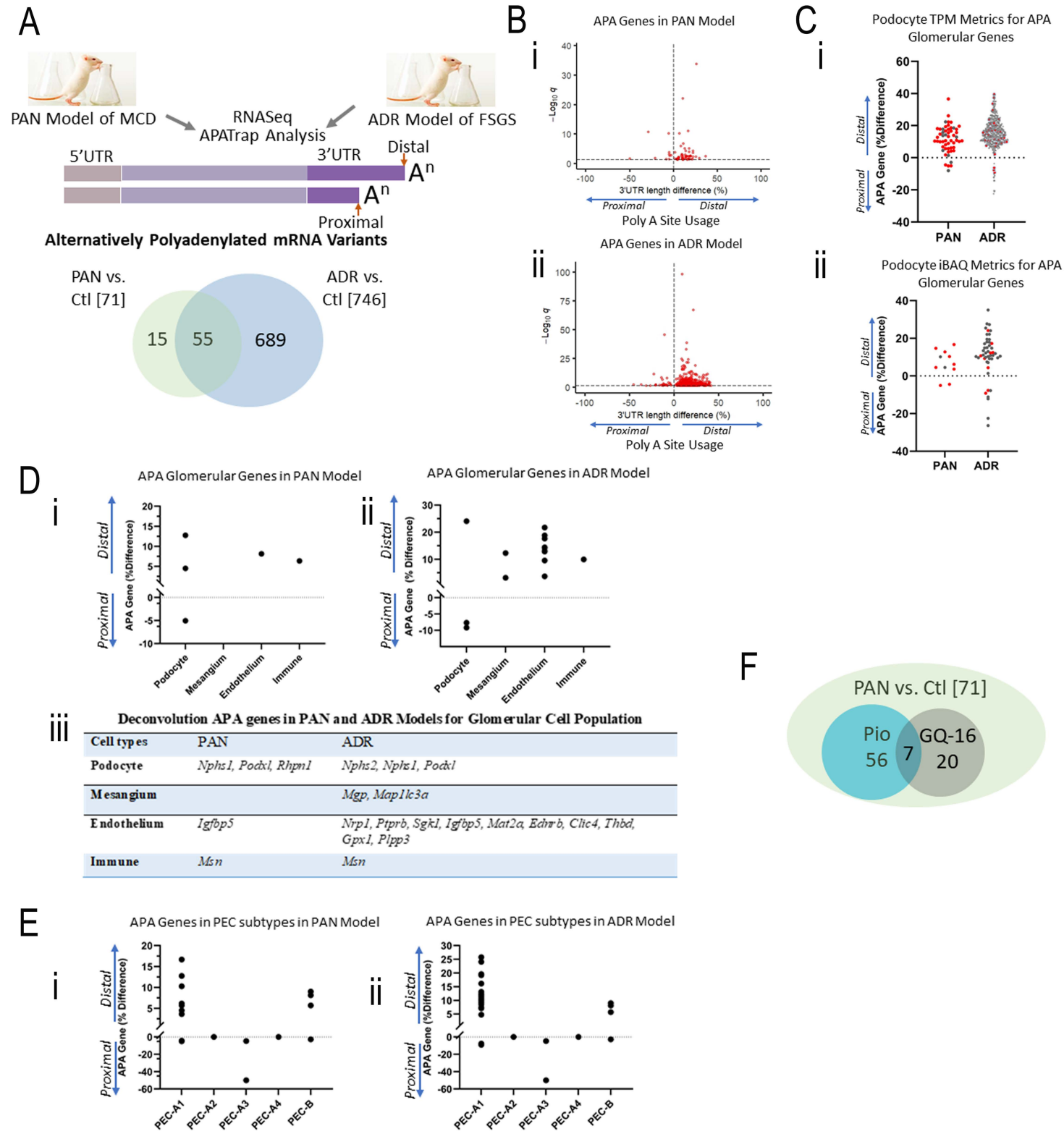

Deconvolution APA genes in PAN and ADR Models for Glomerular Cell Population

Cell types	PAN	ADR
Podocyte	*Nphs1, Podxl, Rhpn1*	*Nphs2, Nphs1, Podxl*
Mesangium		*Mgp, Map1lc3a*
Endothelium	*Igfbp5*	*Nrp1, Ptprb, Sgkl, Igfbp5, Mat2a, Ednrb, Clic4, Thbd, Gpx1, Plpp3*
Immune	*Msn*	*Msn*

Figure 3

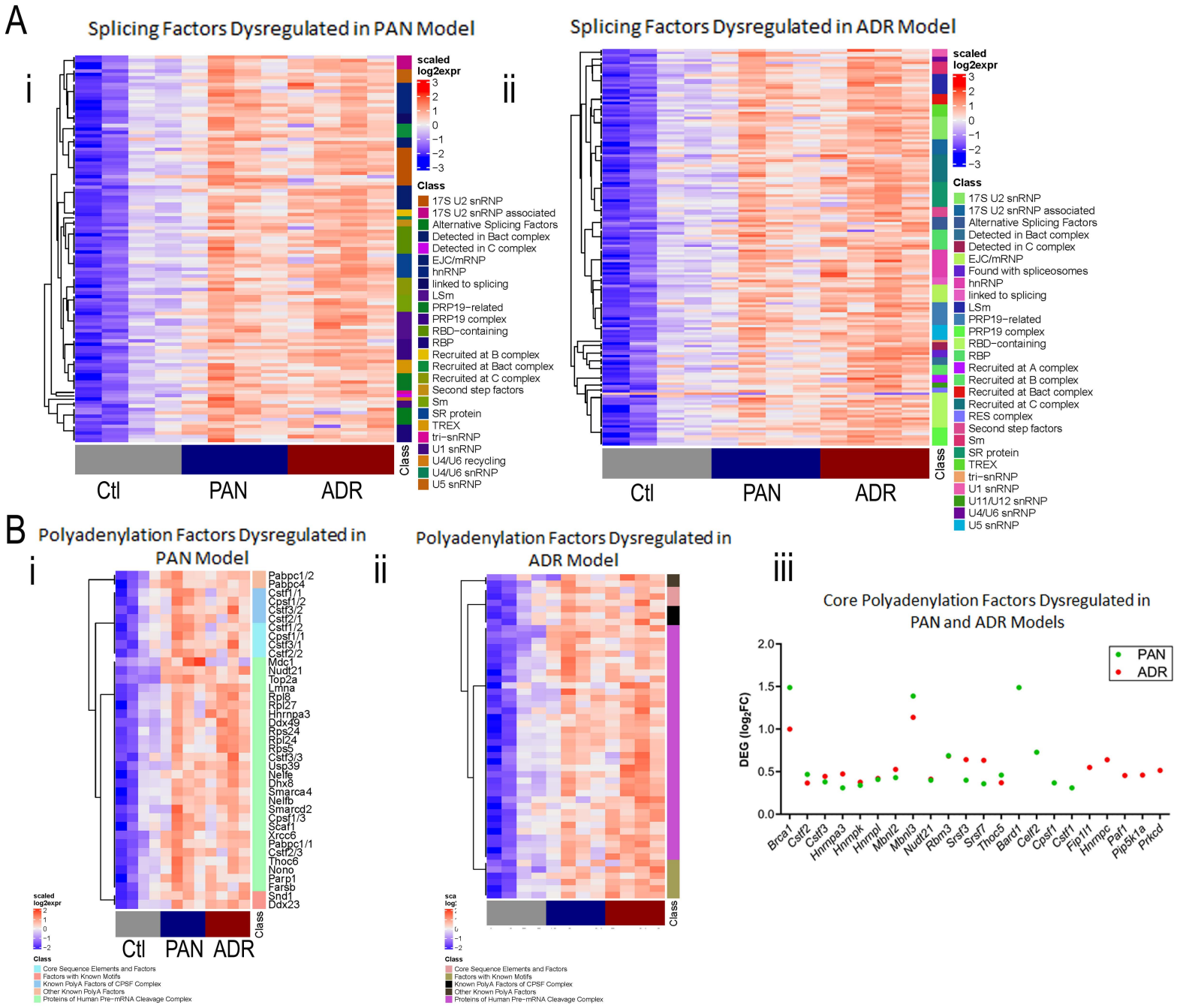
A
Splicing Factors Dysregulated in PAN Model
i
scaled log2expr
3
2
1
0
−1
−2
−3
Class
17S U2 snRNP
17S U2 snRNP associated
Alternative Splicing Factors
Detected in Bact complex
Detected in C complex
EJC/mRNP
hnRNP
linked to splicing
LSm
PRP19−related
PRP19 complex
RBD−containing
RBP
Recruited at B complex
Recruited at Bact complex
Recruited at C complex
Second step factors
Sm
SR protein
TREX
tri−snRNP
U1 snRNP
U4/U6 recycling
U4/U6 snRNP
U5 snRNP
Class
Ctl
PAN
ADR
Splicing Factors Dysregulated in ADR Model
ii
scaled log2expr
3
2
1
0
−1
−2
−3
Class
17S U2 snRNP
17S U2 snRNP associated
Alternative Splicing Factors
Detected in Bact complex
Detected in C complex
EJC/mRNP
Found with spliceosomes
hnRNP
linked to splicing
LSm
PRP19−related
PRP19 complex
RBD−containing
RBP
Recruited at A complex
Recruited at B complex
Recruited at Bact complex
Recruited at C complex
RES complex
Second step factors
Sm
SR protein
TREX
tri−snRNP
U1 snRNP
U11/U12 snRNP
U4/U6 snRNP
U5 snRNP
Class
Ctl
PAN
ADR
B
Polyadenylation Factors Dysregulated in PAN Model
i
Pabpc1/2
Pabpc4
Cstf1/1
Cpsf1/2
Cstf3/2
Cstf2/1
Cstf1/2
Cpsf1/1
Cstf3/1
Cstf2/2
Mdc1
Nudt21
Top2a
Lmna
Rpl8
Rpl27
Hnrnpa3
Ddx49
Rps24
Rpl24
Rps5
Cstf3/3
Usp39
Nelfe
Dhx8
Smarca4
Nelfb
Smarcd2
Cpsf1/3
Scaf1
Xrcc6
Pabpc1/1
Cstf2/3
Thoc6
Nono
Parp1
Farsb
Snd1
Ddx23
scaled log2expr
2
1
0
−1
−2
Class
Ctl
PAN
ADR
Class
Core Sequence Elements and Factors
Factors with Known Motifs
Known PolyA Factors of CPSF Complex
Other Known PolyA Factors
Proteins of Human Pre−mRNA Cleavage Complex
Polyadenylation Factors Dysregulated in ADR Model
ii
Class
Class
Core Sequence Elements and Factors
Factors with Known Motifs
Known PolyA Factors of CPSF Complex
Other Known PolyA Factors
Proteins of Human Pre−mRNA Cleavage Complex
iii
Core Polyadenylation Factors Dysregulated in PAN and ADR Models
PAN
ADR
DEG (log2FC)
2.0
1.5
1.0
0.5
0.0
Brca1
Cstf2
Cstf3
Hnrnpa3
Hnrnpk
Hnrnpl
Mbnl2
Mbnl3
Nudt21
Rbm3
Srsf3
Srsf7
Thoc5
Bard1
Celf2
Cpsf1
Cstf1
Fip1l1
Hnrnpc
Paf1
Pip5k1a
Prkcd

Figure 4

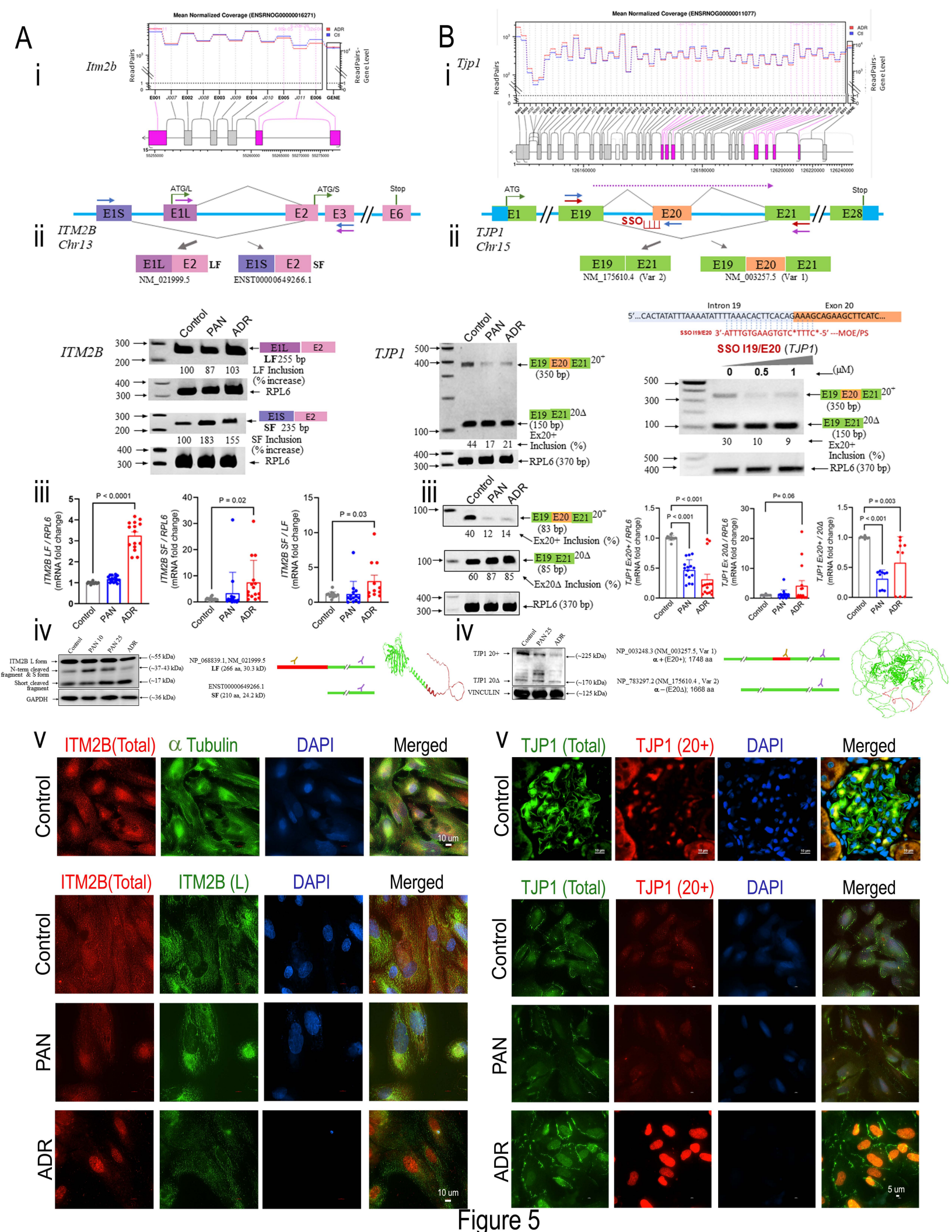
A
i
Itm2b
Mean Normalized Coverage (ENSRNOG00000016271)
ADR
Ctl
ReadPairs
ReadPairs-Gene Level
E001 J007 E002 J008 E003 J009 E004 J010 E005 J011 E006 GENE
ii
ITM2B
Chr13
ATG/L
ATG/S
Stop
E1S
E1L
E2
E3
E6
E1L E2 LF
E1S E2 SF
NM_021999.5
ENST00000649266.1
B
i
Tjp1
Mean Normalized Coverage (ENSRNOG00000011077)
ADR
Ctl
ReadPairs
ReadPairs-Gene Level
ii
TJP1
Chr15
ATG
Stop
E1
E19
E20
E21
E28
SSO
E19 E21
NM_175610.4 (Var 2)
E19 E20 E21
NM_003257.5 (Var 1)
ITM2B
Control
PAN
ADR
300
200
100 87 103
LF Inclusion (% increase)
RPL6
E1L E2
LF 255 bp
400
300
100 183 155
SF Inclusion (% increase)
E1S E2
SF 235 bp
TJP1
500
400
100
E19 E20 E21 20+ (350 bp)
E19 E21 20Δ (150 bp)
44 17 21
Ex20+ Inclusion (%)
RPL6 (370 bp)
Intron 19
Exon 20
5'...CACTATATTTAAAATATTTTAAACACTTCACAGAAAGCAGAAGCTTCATC...
SSO I19/E20 3'-ATTTGTGAAGTGTC*TTTC*-5' ---MOE/PS
SSO I19/E20 (TJP1)
0 0.5 1 (μM)
30 10 9
iii
P < 0.0001
P = 0.02
P = 0.03
ITM2B LF / RPL6 (mRNA fold change)
ITM2B SF / RPL6 (mRNA fold change)
ITM2B SF / LF (mRNA fold change)
Control
PAN
ADR
E19 E20 E21 20+ (83 bp)
40 12 14
Ex20+ Inclusion (%)
E19 E21 20Δ (85 bp)
60 87 85
Ex20Δ Inclusion (%)
P < 0.001
P = 0.06
P = 0.003
TJP1 Ex20+ / RPL6 (mRNA fold change)
TJP1 Ex 20Δ / RPL6 (mRNA fold change)
TJP1 Ex20+ / 20Δ (mRNA fold change)
iv
Control
PAN 10
PAN 25
ADR
ITM2B L form
N-term cleaved fragment & S form
Short cleaved fragment
GAPDH
(~55 kDa)
(~37-43 kDa)
(~17 kDa)
(~36 kDa)
NP_068839.1, NM_021999.5
LF (266 aa, 30.3 kD)
ENST00000649266.1
SF (210 aa, 24.2 kD)
TJP1 20+
TJP1 20Δ
VINCULIN
(~225 kDa)
(~170 kDa)
(~125 kDa)
NP_003248.3 (NM_003257.5, Var 1)
α + (E20+); 1748 aa
NP_783297.2 (NM_175610.4 , Var 2)
α – (E20Δ); 1668 aa
v
ITM2B(Total)
α Tubulin
DAPI
Merged
Control
10 um
ITM2B (L)
PAN
ADR
TJP1 (Total)
TJP1 (20+)
5 um

Figure 5

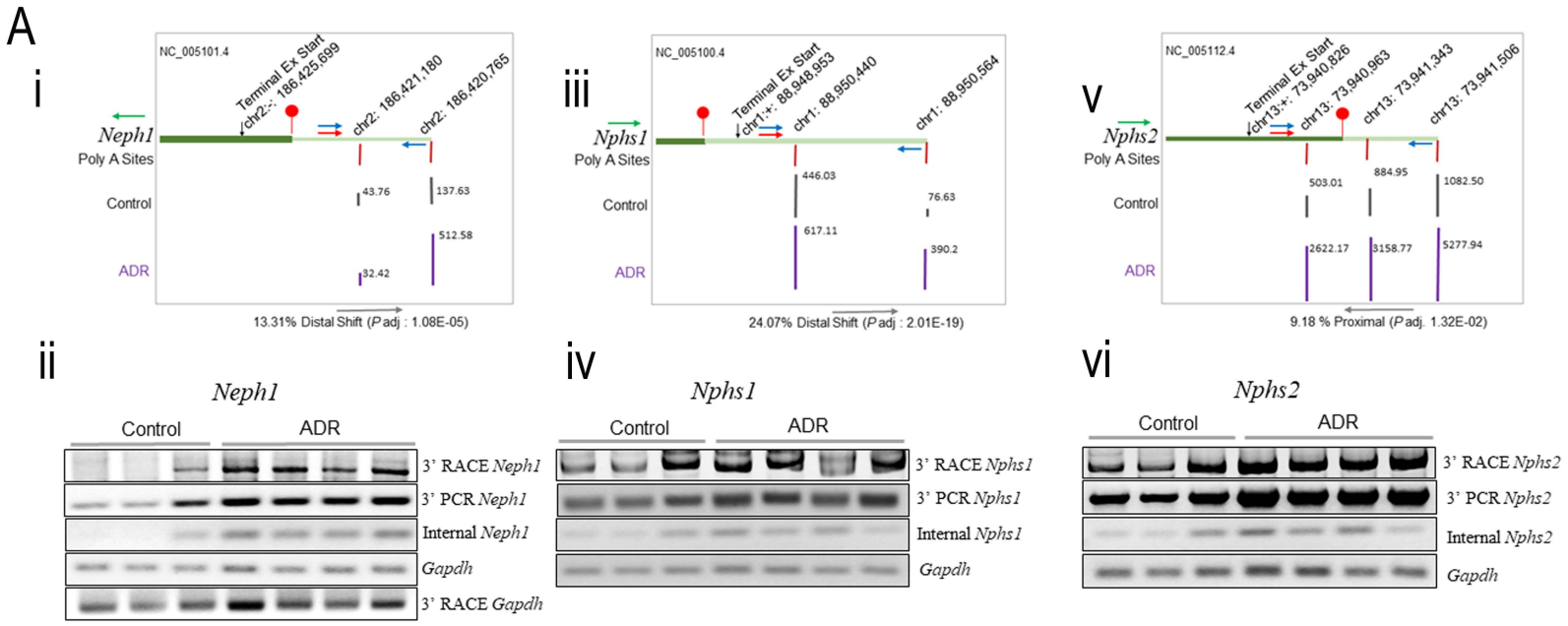
A
i
NC_005101.4
Terminal Ex Start
chr2:-: 186,425,699
chr2: 186,421,180
chr2: 186,420,765
Neph1
Poly A Sites
Control
ADR
43.76
137.63
512.58
32.42
13.31% Distal Shift (Padj : 1.08E-05)
iii
NC_005100.4
Terminal Ex Start
chr1:+: 88,948,953
chr1: 88,950,440
chr1: 88,950,564
Nphs1
Poly A Sites
Control
ADR
446.03
76.63
617.11
390.2
24.07% Distal Shift (Padj : 2.01E-19)
v
NC_005112.4
Terminal Ex Start
chr13:+: 73,940,826
chr13: 73,940,963
chr13: 73,941,343
chr13: 73,941,506
Nphs2
Poly A Sites
Control
ADR
503.01
884.95
1082.50
2622.17
3158.77
5277.94
9.18 % Proximal (Padj. 1.32E-02)
ii
Neph1
Control
ADR
3' RACE Neph1
3' PCR Neph1
Internal Neph1
Gapdh
3' RACE Gapdh
iv
Nphs1
Control
ADR
3' RACE Nphs1
3' PCR Nphs1
Internal Nphs1
Gapdh
vi
Nphs2
Control
ADR
3' RACE Nphs2
3' PCR Nphs2
Internal Nphs2
Gapdh

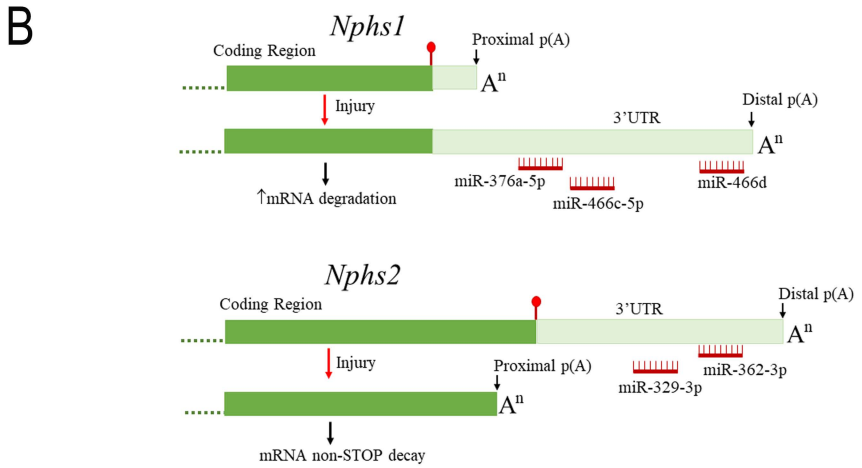
B
Nphs1
Coding Region
Proximal p(A)
Injury
3'UTR
Distal p(A)
↑mRNA degradation
miR-376a-5p
miR-466c-5p
miR-466d
Nphs2
Coding Region
3'UTR
Distal p(A)
Injury
Proximal p(A)
miR-329-3p
miR-362-3p
mRNA non-STOP decay

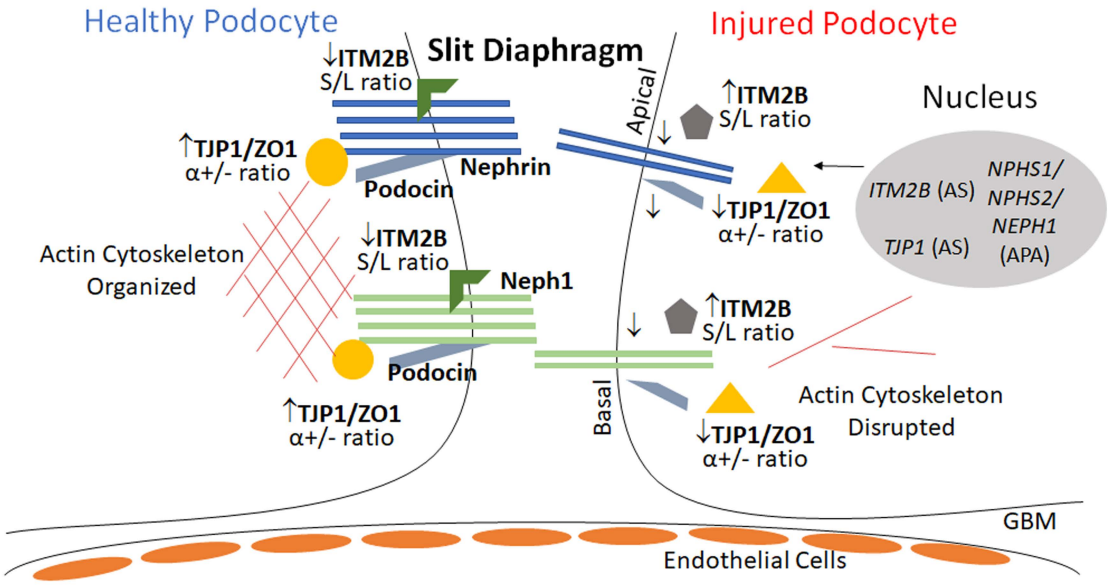
C
Healthy Podocyte
Injured Podocyte
Slit Diaphragm
↓ITM2B
S/L ratio
↑TJP1/ZO1
α+/- ratio
Nephrin
Podocin
Actin Cytoskeleton
Organized
↓ITM2B
S/L ratio
Neph1
Podocin
↑TJP1/ZO1
α+/- ratio
Apical
Basal
↑ITM2B
S/L ratio
↓TJP1/ZO1
α+/- ratio
↑ITM2B
S/L ratio
↓TJP1/ZO1
α+/- ratio
Nucleus
ITM2B (AS)
TJP1 (AS)
NPHS1/
NPHS2/
NEPH1
(APA)
Actin Cytoskeleton
Disrupted
GBM
Endothelial Cells

Figure 6